

# 1 Multi-year high time resolution measurements of fine PM at 13 2 sites of the French Operational Network (CARA program): 3 Data processing and chemical composition

a mis en forme

4 Hasna Chebaicheb<sup>1,2,3</sup>, Joel F. de Brito<sup>1,3</sup>, Tanguy Amodeo<sup>2,3</sup>, Florian Couvidat<sup>2</sup>, Jean-Eudes  
5 Petit<sup>4</sup>, Emmanuel Tison<sup>1,3</sup>, Gregory Abbou<sup>5</sup>, Alexia Baudic<sup>5</sup>, Mélodie Chatain<sup>6</sup>, Benjamin  
6 Chazeau<sup>7,8</sup>, Nicolas Marchand<sup>8</sup>, Raphaële Falhun<sup>9</sup>, Florie Francony<sup>10</sup>, Cyril Ratier<sup>10</sup>, Didier  
7 Grenier<sup>11</sup>, Romain Vidaud<sup>11</sup>, Shouwen Zhang<sup>12</sup>, Gregory Gille<sup>13</sup>, Laurent Meunier<sup>2,3</sup>, Caroline  
8 Marchand<sup>2,3</sup>, Véronique Riffault<sup>1,3</sup>, Olivier Favez<sup>2,3</sup>

a mis en forme : Français (France)

9 <sup>1</sup>IMT Nord Europe, Institut Mines-Télécom, Université de Lille, Centre for Energy and Environment, 59000, Lille,  
10 France

11 <sup>2</sup>Institut National de l'environnement Industriel et des Risques (INERIS), 60550 Verneuil-en-Halatte, France

12 <sup>3</sup>Laboratoire Central de Surveillance de la Qualité de l'Air (LCSQA), 60550 Verneuil-en-Halatte, France

13 <sup>4</sup>Laboratoire des Sciences du Climat et de l'Environnement (LSCE), CNRS-CEA-UVSQ (UMR 8212), 91191 Gif-  
14 sur-Yvette, France

15 <sup>5</sup>Airparif, Air Quality Monitoring Network for the Greater Paris Area, 75004 Paris, France

16 <sup>6</sup>Atmo Grand Est, 67300 Schiltigheim, France

17 <sup>7</sup>Laboratory of Atmospheric Chemistry, Paul Scherrer Institute, 5232 Villigen, Switzerland

18 <sup>8</sup>Aix Marseille Univ, CNRS, LCE, Marseille, France

19 <sup>9</sup>Air Breizh, 35200 Rennes, France

20 <sup>10</sup>Atmo Nouvelle-Aquitaine, 33692 Mérignac, France

21 <sup>11</sup>Atmo Auvergne Rhône-Alpes, 69500 Bron, France

22 <sup>12</sup>Atmo Hauts-de-France, 59800 Lille, France

23 <sup>13</sup>AtmoSud, Regional Network for Air Quality Monitoring of Provence-Alpes-Côte-d'Azur, Marseille, France

a mis en forme : Français (France)

25 *Correspondence to:* hasna.chebaicheb@ineris.fr

26  
27 **Abstract.** This paper presents a first comprehensive analysis of long-term measurements of atmospheric aerosol  
28 components from Aerosol Chemical Speciation Monitor (ACSM) and multi-wavelength Aethalometer (AE33)  
29 instruments collected between 2015 and 2021 at 13 (sub)urban sites as part of the French CARA program. The  
30 datasets contain the mass concentrations of major chemical species within PM<sub>1</sub>, namely organic aerosols (OA),  
31 nitrate (NO<sub>3</sub><sup>-</sup>), ammonium (NH<sub>4</sub><sup>+</sup>), sulfate (SO<sub>4</sub><sup>2-</sup>), non-sea-salt chloride (Cl<sup>-</sup>), and equivalent black carbon (eBC).  
32 Rigorous quality control, technical validation, and environmental evaluation processes were applied, adhering to  
33 both the guidance from the French reference laboratory for air quality monitoring and the Aerosol, Clouds, and  
34 Trace gases Research Infrastructure (ACTRIS) standard operating procedures. Key findings include geographical  
35 differences in aerosol chemical composition, seasonal variations, and diel patterns, which are influenced by  
36 meteorological conditions, anthropogenic activities, and proximity to emission sources. Overall, OA dominates  
37 PM<sub>1</sub> at each site (43-60 % of total mass), showing distinct seasonality with higher concentrations (i) in winter,  
38 due to enhanced residential heating emissions, and (ii) in summer, due to increased photochemistry favoring  
39 secondary aerosol formation. NO<sub>3</sub> is the second most important contributor to PM<sub>1</sub> (15-30 %), peaking in late  
40 winter and early spring, especially in northern France, and playing a significant role during pollution episodes.  
41 SO<sub>4</sub> (8-14 %) and eBC (5-11 %) complement the major fine aerosol species, with their relative contributions  
42 strongly influenced by the origin of air masses and the stability of meteorological conditions, respectively.

43 ~~Such chemically-speciated multi-year datasets have significant value for the scientific community, offering~~  
44 ~~opportunities for future research, including source apportionment studies, trend analyses, and epidemiological~~  
45 ~~investigations. They are also vital for evaluating and validating regional air quality models. In this regard, a~~  
46 ~~comparison with the CHIMERE Chemical Transport Model~~A comparison with the 3D Chemical Transport Model  
47 (CTM) CHIMERE shows high correlations between simulations and measurements, albeit underestimating OA  
48 concentrations by 46-76 %. Regional discrepancies in NO<sub>3</sub> concentration levels emphasize the importance of these  
49 datasets in validating air quality models and tailoring air pollution mitigation strategies.

50 **Keywords.** Urban pollution, ACSM, AE33, equivalent black carbon eBC, non-refractory submicron aerosols NR-  
51 PM<sub>1</sub>, Chemical composition, France, chemical transport model/modeling

## 1 Introduction

The investigation of atmospheric aerosols holds significant importance in both the scientific and policy spheres due to their substantial impacts on climate (IPCC, 2021) and human health (WHO, 2021). In Europe, for instance, it is estimated that in 2021, 97 % of the urban population experienced levels surpassing the annual concentration of  $5 \mu\text{g m}^{-3}$  recommended by the World Health Organization (WHO) for particulate matter with an aerodynamic diameter smaller than  $2.5 \mu\text{m}$  ( $\text{PM}_{2.5}$ ), and exposure to these fine particles was associated in 2021 with more than 253,000 premature deaths (EEA, 2023). WHO guidelines as well as regulatory thresholds set at the national level (according to the Directive 2008/50/EC for European Member States) are mainly linked with the total mass concentration of suspended particles in a given size range. However, the elaboration and evaluation of specific action plans to improve air quality require a sound knowledge of their formation, which also allows the investigation of their emission sources and chemical processes in ambient air (Viana et al., 2008, Fuzzi et al., 2015). Moreover, forecasting systems, such as those using Chemical Transport Models (CTMs), usually use chemically-speciated emission inventories as inputs, and their validation benefits from comparisons with measurements of the PM chemical composition at representative sites (e.g., Ciarelli et al., 2016, EMEP, 2022).

Historically, PM chemical speciation was mainly based on offline laboratory analyses of aerosol samples collected on filters (e.g., Putaud et al., 2004). Such methods are nowadays well standardized and provide the opportunity for comprehensive characterization of major species as well as trace compounds (EMEP, 2022). However, they are known to be subject to various sampling artifacts (Schaap et al., 2004; Wittmaack and Keck, 2004) and are collected at relatively low temporal resolution (typically 24h). They are also quite laborious and costly when used for long-term monitoring purposes. To overcome these limitations, significant efforts have been made to develop online chemical analyzers for in situ measurements in near real time. In particular, there has been a growing interest in the continuous quantification of black carbon in ambient air, especially using filter-based absorption photometers (Savadkoobi et al., 2023), given the significant influence of this aerosol component on climate (Jacobson and Forster et al., 2001-2023). In parallel, the development and worldwide deployment in the last two decades of the Aerosol Mass Spectrometer (AMS, Canagaratna et al., 2007) has allowed studying non-refractory compounds (i.e., organic aerosol (OA), nitrate ( $\text{NO}_3^-$ ), sulfate ( $\text{SO}_4^{2-}$ ), chloride ( $\text{Cl}^-$ ), and ammonium ( $\text{NH}_4^+$ )) within the fine aerosol mode (mainly  $\text{PM}_{10}$ ) (Crenn et al., 2017, Lanz et al., 2010, Roig Rodelas et al., 2019, Sun et al., 2010, Zhang et al., 2017). In addition to these sophisticated high-resolution instruments, which are well suited for intensive but short-term campaigns, the Aerosol Chemical Speciation Monitor (ACSM) has been designed for continuous, multiannual measurements of the same major chemical species in the  $\text{PM}_{10}$  or  $\text{PM}_{2.5}$  fractions (Bressi et al., 2021; Chebaicheb et al., 2023; Heikkinen et al., 2021; Ng et al., 2011; Zhang et al., 2019). Both measurement methods (i.e., absorption photometers and ACSM) have become widely used in research monitoring, such as the Aerosol, Clouds, and Trace gases Research Infrastructure (ACTRIS, [www.actris.eu](http://www.actris.eu)) in Europe (Laj et al., 2024), and within the Atmospheric Science and mEasurement NeTwork (ASCENT, <https://research.gatech.edu/>) in the United States. Their robustness and relatively low operating costs also make them good candidates for deployment at air quality monitoring stations operated by environmental agencies (Petit et al., 2015).

In this context, since 2015, multi-wavelength Aethalometers (AE33 model, Drinovec et al., 2015) and ACSM instruments have been operated at an increasing number of urban sites in France as part of the CARA program

a mis en forme : Bordure : Bas: (Pas de bordure)

91 [\(Chemical characterization of particulate matter, set up in 2008 by the French reference laboratory for air quality](#)  
92 [monitoring\)](#) within the national air quality monitoring network (Favez et al., 2021), with the following main  
93 objectives: (i) to document in near real time the chemical composition (and possibly the dominant sources) of PM  
94 pollution episodes; (ii) to provide multi-year datasets of the chemical composition of the fine PM fraction, to be  
95 included into future trend analyses and/or epidemiological studies; (iii) to provide a comprehensive overview of  
96 the temporal and spatial variability of the chemical composition of fine PM over France, which can contribute in  
97 particular to evaluating and improving the accuracy of air quality models.

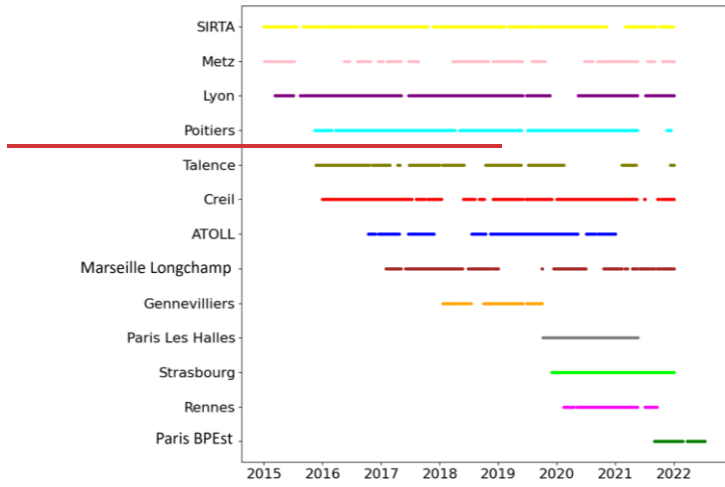
98 The main objective of this paper is to report on the chemically-specified [multi-year](#) datasets and major findings  
99 obtained so far from these observations. After describing the quality control procedures applied to the  
100 corresponding measurements, we investigate the geographical specificities exhibited by the main chemical species  
101 within the fine PM and then provide typical seasonal and diel variations displayed by these compounds in France  
102 over the period 2015-2021. The datasets presented here are made fully available for complementary research  
103 activities, including [the evaluation of the accuracy of CTM trend analyses and epidemiological investigations.](#)  
104 [They are also vital for evaluating and validating regional air quality models](#) through comparison exercises,  
105 examples of which are also discussed in this article [using CHIMERE CTM model simulations. Indeed, the](#)  
106 [CHIMERE model is routinely validated against observations, and the online data from the CARA program play a](#)  
107 [crucial role in France for the continuous enhancement of CHIMERE, resulting in more accurate forecasts.](#)

## 108 2 Methodology

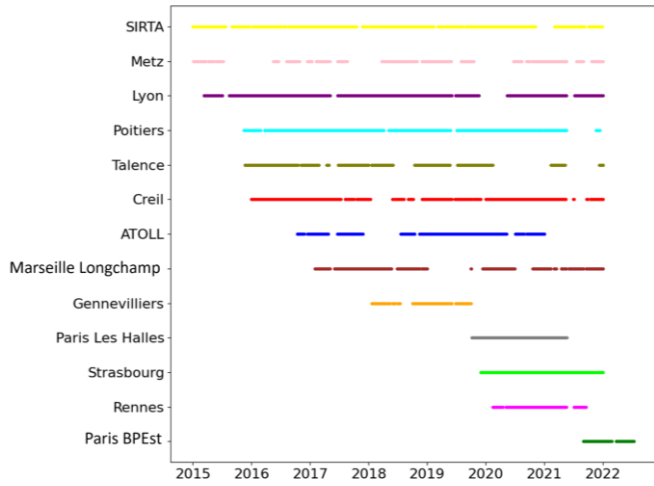
### 109 2.1 Sites and measurement periods

110 The current study presents the chemical composition of fine particles within the CARA program during the period  
111 2015-2021, at 13 sites in France, including 11 stations from regional air quality monitoring networks (AASQAs),  
112 as well as two research platforms - i.e., SIRTA (Greater Paris area) and ATOLL (Lille metropolis) - both of which  
113 are also part of the ACTRIS European research infrastructure. These stations have been gradually equipped with  
114 AE33 and ACSM instruments from 2015 onwards. [A detailed description of these A one-year \(2016-2017\) dataset](#)  
115 [of ACSM measurements for ATOLL \(Lille\), SIRTA \(Paris\), and Marseille Longchamp was previously integrated](#)  
116 [into a multi-site European study \(Chen et al., 2022\). A detailed description of the](#) instruments is given in the next  
117 section, and the temporal coverage of the measurements considered here for each site is presented in Figure 1. A  
118 summary of each sampling site, including coordinates and related networks, can also be found in the  
119 Supplementary Information, Table S1. The majority of these sites are urban background sites, with the exception  
120 of two suburban sites (ATOLL and SIRTA) and one urban traffic site (Boulevard Périphérique Est; BPEst in Paris).  
121 Geographically distributed throughout France, these sampling sites provide a global view of the chemical  
122 composition of fine particles at the national scale.

a mis en forme : Bordure : Bas: (Pas de bordure)



124



125

126 **Figure 1: ACSM and AE33 measurement periods considered for each site in this study.**

a mis en forme : Police :10 pt, Non Gras

127

128 **2.2 Non-refractory submicron aerosol measurements**

129 **2.2.1 ACSM measurement principles**

130 The ACSM, developed by Aerodyne Research Inc., is based on mass spectrometry. As previously mentioned, it  
 131 measures the chemical composition of non-refractory submicron aerosols NR-PM<sub>1</sub> in real-time, allowing long-

132 term measurements with less monitoring and technical intervention compared to AMS, and a relatively high  
133 temporal resolution of about 30 minutes (Watson, 2017). All stations presented in this study are equipped with  
134 Quadrupole ACSMs (Q-ACSM, Ng et al., 2011), except for the Marseille-Longchamp site, where a Time-of-flight  
135 ACSM (ToF-ACSM, Fröhlich et al., 2013) is deployed. The Q-ACSM is the most commonly used analyzer  
136 because it meets the operational monitoring needs of the French monitoring agencies and is less complex than the  
137 ToF-ACSM, although the latter has lower detection limits and slightly better time resolution (about 10 minutes).  
138 [More information about these instruments is presented in Table S2.](#)

139 The operating principle of the ACSM is briefly described below. Ambient air first enters the vacuum system  
140 through a 100  $\mu\text{m}$  diameter critical orifice. It then passes through an aerodynamic lens that focuses the aerosol into  
141 a concentrated beam, which is further directed onto a vaporizer heated at a temperature of about 600°C, causing  
142 the particles to transition to the gas phase. The gas phase molecules are then subjected to ionization at 70 eV,  
143 resulting in molecular fragmentation. The fragmented ions are guided by ion lenses to a quadrupole or time-of-  
144 flight mass filter, depending on the ACSM model.

145 In the ACSM, the atmospheric sample is analyzed alternatively by passing or not through a particulate filter. The  
146 air signal can thus be subtracted from the unfiltered measurements to quantify the particulate chemical species. A  
147 measurement timebase of approximately 29 min (corresponding to 28 cycles of filtered/unfiltered atmospheric  
148 samples) was used for each Q-ACSM dataset, while data were acquired with a 10 min timebase for the ToF-  
149 ACSM. All ACSMs operated under the CARA program were equipped with a  $\text{PM}_{10}$  aerodynamic lens and a  
150 standard vaporizer.

151 In the measured mass spectra, each  $m/z$  fragment is linked to one or more species based on a fragmentation table  
152 originally developed by Allan et al. (2004) and subsequently refined by Canagaratna et al. (2007). The  
153 concentration of each chemical species is then obtained as the sum of its contribution in every corresponding  $m/z$   
154 fragment. Moreover, the instrument-specific response factor (RF) of  $\text{NO}_3$  and the relative ionization efficiencies  
155 (RIE) of  $\text{NH}_4$  and  $\text{SO}_4$  are determined by sampling 300 nm ammonium nitrate ( $\text{NH}_4\text{NO}_3$ ) and ammonium sulfate  
156 ( $(\text{NH}_4)_2\text{SO}_4$ ) aerosols (Freney et al., 2019). For OA and Cl, the default RIE values of 1.4 and 1.3 are used here.  
157 Finally, to obtain quantitative mass concentrations for each measured chemical species, a collection efficiency  
158 (CE) correction factor is applied, following the procedure proposed by Middlebrook et al. (2011) [as discussed](#)  
159 [below.](#)

### 160 2.2.2 ACSM quality checks and data handling

161 The data collected here from the ACSM instrument follows strict quality control and technical validation, including  
162 an environmental evaluation involving comparison with complementary data. It has been performed following the  
163 guidance provided by the French reference laboratory for air quality monitoring (LCSQA, 2018) and in full  
164 agreement with the ACTRIS standard operating procedures, which are available online (<https://www.actris-ecac.eu/pmc-non-refractory-organics-and-inorganics.html>).

166 On-site calibrations for air quality monitoring sites have been performed yearly by LCSQA personnel as well as  
167 after each sensitive maintenance by the instrument distributor in Europe (ADDAIR). A detailed description of the  
168 applied calibration procedures is available in a specific document edited at the national level (LCSQA, 2022).  
169 Moreover, each ACSM of the CARA program has routinely participated in intercomparison exercises organized

170 by the Aerosol Chemical Monitor Calibration Centre (ACMCC) at SIRTA, to ensure proper calibration and  
171 functioning of the instruments (e.g., LCSQA, 2023).

172 Given the majority of instruments used here are Q-ACSM, data processing will be detailed focusing on this model.  
173 ToF-ACSM data processing (deployed at Marseille-Longchamps) is described more specifically in Chazeau et al.  
174 (2021). The Q-ACSM data handling was carried out using the manufacturer's software in Igor Pro Version 6.37.  
175 The first step involved checking the stability and continuity of technical parameters, including inlet pressure  
176 (maintained at approximately  $1.3 \pm 0.2$  torr), vaporizer temperature (regulated from the voltage calibration curve  
177 initially defined by the manufacturer), Secondary Electron Multiplier (SEM) and Heater Bias voltages, filament  
178 emission, airbeam value (set around  $10^7 \pm 30\%$  ions/s), and relative humidity (ensuring it remains below 40 %  
179 using a Nafion dryer upstream the inlet). Data points exhibiting inconsistencies were systematically flagged and  
180 invalidated. Secondly, the calibration results, notably the RF and RIE, were carefully analyzed for consistency.  
181 This approach ensured that the data cleaning process was attuned to changes in RF and RIE, thereby improving  
182 the accuracy of the resulting dataset. If the RIE and RF values from two subsequent calibrations were deemed  
183 comparable, their average was used. Otherwise, time-dependent RIE and RF were used, notably following  
184 instrument modification. During this data cleaning phase, the CE was maintained at a constant value of 1. Thirdly,  
185 data points with air (m/z 28, 32, and 40) and water (m/z 18) signal spikes were removed through a systematic  
186 cleaning procedure executed within the Igor Pro software, which allows the removal of signals that appear  
187 anomalous. This step also entails a comprehensive analysis of other ions to capture additional insights from the  
188 data. In particular, the examination of ions associated with chloride (m/z 35 and 36) allows for checking any  
189 possible measurement artifact that may be caused by sea salts (Tobler et al., 2020), while specific organic  
190 compounds (m/z 43, 44, and 55), including the fragment related to levoglucosan (m/z 60), serve as a crucial  
191 checkpoint for assessing the impact of distinct sources, such as biomass combustion, traffic emissions and/or  
192 secondary formation processes.

193 As a next step, the implementation of the TIS (*Time series*) and RIT (*Relative Ion Transmission*) corrections were  
194 performed. The TIS correction encompasses the correction of crucial time-dependent signals that exert a significant  
195 influence on the measured concentrations captured by the instrument. These include the adjustment of variables  
196 such as the inflow rate directed into the Q-ACSM 'reference P' (inlet pressure), the 'reference N2' signal for  
197 airbeam, and the 'reference RF' for ionization efficiency. Subsequently, the RIT correction is applied to account  
198 for the mass spectrometer transmission efficiency within the Q-ACSM, based on the naphthalene peaks used as  
199 internal standard and represented by m/z 51, 62, 76, 102, and 128 (normalized to 1 below m/z -51 and set at 0.05  
200 for m/z 154 and beyond with an exponential fit for the interval in between). We also closely examined the RIT  
201 time series linked to these ions, particularly in cases where the RIT standard deviation was high. We found several  
202 instances where the mean RIT value may appear satisfactory, yet the time series could have periods of anomalous  
203 behavior. Thus, it is essential to carefully examine each time series of individual naphthalene masses, beyond the  
204 evaluation of average RIT values alone. After these corrections, the Middlebrook algorithm (Middlebrook et al.,  
205 2011), with a minimum CE of 0.5, was applied to correct the mass concentrations for the so-called composition-  
206 dependent collection efficiency (CDCE) correction.

207 The following verification step involves examining the ion balance, which implies assessing the correlation  
208 between the measured and predicted  $\text{NH}_4$  concentrations, with a target slope theoretically falling within the range

209 of  $1 \pm 10\%$ , at sites and under atmospheric conditions where most aerosols should contain enough ammonium to  
210 be neutral as ammonium nitrate  $\text{NH}_4\text{NO}_3$ , ammonium sulfate  $(\text{NH}_4)_2\text{SO}_4$  and ammonium chloride  $\text{NH}_4\text{Cl}$ . To  
211 compute the measured and predicted  $\text{NH}_4$  concentrations, the following calculations were employed:

$$212 \quad \text{NH}_{4,\text{measured}} = \frac{[\text{NH}_4]}{18} \quad (1)$$

$$213 \quad \text{NH}_{4,\text{predicted}} = \frac{[\text{NO}_3]}{62} + 2 \frac{[\text{SO}_4]}{96} + \frac{[\text{Cl}]}{35.45} \quad (2)$$

214 Finally, the analysis carefully accounted for the specific detection limits (DL) corresponding to various chemical  
215 species. Following Ng et al. (2011a), DL values for Q-ACSM are 0.284, 0.148, 0.024, 0.012, and  $0.011 \mu\text{g m}^{-3}$   
216 for  $\text{NH}_4$ , OA,  $\text{SO}_4$ ,  $\text{NO}_3$ , and Cl, respectively. The same DL has been considered here for the ToF-ACSM  
217 instrument deployed in Marseille-Longchamp. Data levels above the DL were validated, whereas those between -  
218  $3 \times \text{DL}$  and DL were replaced by  $\text{DL}/2$ . Conversely, data below  $-3 \times \text{DL}$  were invalidated (Table [S2S3](#)).

219

## 220 **2.3 Equivalent Black Carbon measurements**

### 221 **2.3.1. Brief description of the AE33 device**

222 Complementary to ACSM measurements, equivalent black carbon (eBC) has been monitored at all sites over the  
223 same periods using a multi-wavelength Aethalometer model AE33 (Magee Scientific). As with other filter-based  
224 absorption photometers, the AE33 primarily determines aerosol absorption coefficients ( $b_{\text{abs}}$ ) at selected  
225 wavelengths, based on the rate of change in the attenuation of light transmitted through the particle-laden filter. A  
226 full description of the AE33 operating principles is given by Drinovec et al. (2015). Briefly, the instrument  
227 continuously captures aerosol particles by directing the airflow onto a specific spot on the filter tape. It assesses  
228 the aerosol by gauging the amount of light transmission that passes through a part of the filter tape containing the  
229 sample, compared to the light passing through a reference zone. In the AE33, the reference zone also samples  
230 aerosols albeit with a reduced airflow, thus at different aerosol accumulation rates, allowing for more accurate  
231 eBC and particle light absorption estimates (termed 'dual spot'). The analysis is carried out at seven optical  
232 wavelengths ranging from near-ultraviolet (UV) to near-infrared (IR) (370, 470, 525, 590, 660, 880, and 950 nm).

233 It should be noted that AE33 measurements used in the present paper have been performed in the  $\text{PM}_{10}$  fraction at  
234 both ACTRIS national facilities (ATOLL and SIRTA) but in the  $\text{PM}_{2.5}$  fraction at other stations. It is however  
235 considered that black carbon aerosols are overwhelmingly present in submicron particle matter (Bond et al., 2013)  
236 so that eBC concentrations discussed herewith can be (i) compared together (i.e., from one site to another), and  
237 (ii) combined with ACSM NR- $\text{PM}_{10}$  measurements to describe the main chemical components of fine PM at the  
238 studied sites.



### 239 2.3.2. AE33 quality checks and data handling

240 Similarly to ACSM measurements, the AE33 devices were operated following the LCSQA guidelines (LCSQA,  
241 2020). The absorption coefficients used herewith were then calculated at each wavelength according to current  
242 ACTRIS guidelines (<https://actris-ecac.eu/particle-light-absorption.html>), following Eq. (3):

$$243 \quad b_{abs} = \frac{eBC \times MAE}{H} \quad (3)$$

244 where MAE represents the specific mass absorption efficiency corresponding to each wavelength (empirically  
245 determined by the manufacturer), and H is the appropriate harmonization factor to account for multiple scattering  
246 effects of the filter, which is set at 1.76 for AE33 devices using the M8060 filter tape. The eBC concentrations  
247 were then derived by normalization with a constant mass absorption cross-section ( $MAC_{ACTRIS}$ ) recently  
248 investigated in the frame of the H2020 RI-URBANS EU research program (Alastuey et al., 2022; Savadkoobi et  
249 al., 2023, 2024), following Eq. (4):

$$250 \quad eBC = \frac{b_{abs}}{MAC_{ACTRIS}} \quad (4)$$

251 eBC concentrations are obtained at a wavelength of 880 nm, ~~which is recommended for black carbon~~  
252 ~~measurements. This is because where~~ it is less prone to artifacts caused by other light-absorbing compounds such  
253 as dust ~~and (notably iron oxides) and some~~ organic compounds (~~notably iron oxides and termed~~ brown carbon, BrC,  
254 which absorb light at shorter wavelengths in the UV spectrum). ~~In ambient air, the MAC value varies from site to~~  
255 ~~site and from season to season, which affects the quantification of eBC mass concentrations. The harmonization~~  
256 ~~factor was introduced by ACTRIS to standardize the calculation of absorption coefficients, depending on the filter~~  
257 ~~tape used.~~ At 880 nm, the  $MAC_{ACTRIS}$  factor used here is equivalent to  $7.5 \text{ m}^2 \text{ g}^{-1}$ , also in good agreement with  
258 results previously obtained by Zanatta et al. (2016). It should be noted nonetheless that the application of the  
259 harmonization factor and the subsequent recalculation of eBC using a ~~default and constant~~ MAC ~~comparable to~~  
260 ~~the one applied by the manufacturer results value result~~ in a ~~41% reduction in~~ ~~of about 40 % for~~ eBC levels  
261 compared to ~~the instrument output and reentrain outputs widely used in previous pan-European~~ studies (~~e.g. such~~  
262 ~~as~~ Chen et al., 2022).

263 AE33 data qualification procedures include checking the AAE value obtained from the seven wavelengths for each  
264 data point, aggregated to a 15 min time base. Lower and upper acceptable AAE values of 0.7 and 3.0 are ~~arbitrarily~~  
265 considered here, and the determination coefficient ( $r^2$ ) of the exponential fit used to calculate this AAE value must  
266 be greater than 0.9. Datapoints that did not meet these criteria were discarded. The ~~carefully~~-validated data also  
267 underwent ~~a thorough~~ assessment against the instrumental DL, which was set at approximately  $100 \text{ ng m}^{-3}$ . Data  
268 falling within the range of  $-3 \times DL$  to  $DL$  were replaced by  $DL/2$ , and data below  $-3 \times DL$  were invalidated (Table  
269 ~~S2S3~~).

270  
271 The source apportionment of ambient eBC concentrations is based on the model of Sandradewi et al., (2008).  
272 Briefly, the two-component model calculates the aerosol optical absorption coefficient by combining fractions  
273 associated with wood burning (wb) and fossil fuel (ff) combustion. It exploits the variations in absorption  
274 characteristics at different wavelengths. This method is based on the assumption that wood combustion has a  
275 marked absorption in the UV (high AAE) compared with fossil fuels (low AAE). For this study, and the different

276 sites, the separation between eBC<sub>fr</sub> and eBC<sub>wb</sub> was performed using the values provided by the AE33 manufacturer:  
277 AAE<sub>fr</sub> = 1 and AAE<sub>wb</sub> = 2 (Drinovec et al., 2015).

#### 278 **2.4 Chemical mass closure and related uncertainties**

279 PM<sub>1</sub> is a significant fraction of PM<sub>2.5</sub> especially in Europe (Putaud et al., 2004), understanding the composition  
280 and concentration of PM<sub>1</sub> is therefore essential for assessing the health risks and wider environmental impacts  
281 associated with PM<sub>2.5</sub> exposure. PM<sub>1</sub> mass was reconstructed from combining chemical species from ACSM (non-  
282 refractory NR-PM<sub>1</sub> = OA + NO<sub>3</sub> + SO<sub>4</sub> + NH<sub>4</sub> + Cl) and eBC from AE33 (PM<sub>1</sub> = NR-PM<sub>1</sub> + eBC). For each station  
283 over the study period, PM<sub>1</sub> ~~mass~~ concentrations were compared with continuous PM<sub>2.5</sub> measurements  
284 conducted using a tapered element oscillating microbalance equipped with the filter dynamic measurement system  
285 (TEOM-FDMS; Thermo Fisher Scientific) and/or a FIDAS 200 optical particle counter (Palas GmbH) and/or a β  
286 gauge monitor (BAM 1020; MET ONE), according to the European standard for PM regulatory measurements  
287 (EN 16450).

288 Linear regressions of hourly data reveal fairly good agreement between the reconstructed PM<sub>1</sub> and the PM<sub>2.5</sub> mass  
289 concentrations measured at each site (Figure S1), with determination coefficients (r<sup>2</sup>) ranging from 0.72 to 0.88  
290 (except for Marseille-Longchamp, which yielded an r<sup>2</sup> value of 0.58) and slopes varying from 0.71 to 0.99 (except  
291 for Lyon, Strasbourg, and Metz, which showed distinct lower slopes of 0.57, 0.58, and 0.61, respectively). These  
292 results confirm that PM<sub>2.5</sub> are predominantly made up of submicron particles and underscore the ACSM efficacy  
293 in capturing a significant proportion of that fraction at most sites. Hereafter, PM<sub>1</sub> (mass concentration) will be used  
294 to refer to submicron aerosol loadings estimated as the sum of eBC and NR-PM<sub>1</sub> species measured by the AE33  
295 and ACSM, respectively.

#### 296 **2.5 The CHIMERE model**

297 ~~In order to compare the PM<sub>1</sub> species measurements and results obtained with a CTM, 3D simulations were~~  
298 ~~performed from a recent version of the CHIMERE model (Menut et al., 2021) coupled with the SSH aerosol v1.3~~  
299 ~~aerosol model (Sartelet et al., 2020). One important feature of SSH aerosol consists in the computation of gas-~~  
300 ~~partiele partitioning with the thermodynamic module SOAP (Couvidat et al., 2015). This model~~ Reconstructed PM<sub>1</sub>  
301 may overestimate measured PM<sub>2.5</sub> loadings mainly due to the respective measurement uncertainties of each  
302 technique used here. For PM<sub>2.5</sub>, the FIDAS instrument has been demonstrated as equivalent to the EN12341  
303 standard method with a maximum overall uncertainty of 25 % compared to this reference method according to  
304 EN16450 (Amodeo, 2024). It should also be stated that this instrument is sensitive to particles above 180 nm  
305 optical diameter only, which may result in even higher uncertainties for the estimation of the PM<sub>1</sub> mass fraction.  
306 For eBC, a recent intercomparison between 23 AE33 devices (Cuesta-Mosquera et al., 2021) in the framework of  
307 the ACTRIS research infrastructure showed that the total mean deviation of the eBC concentrations at 880 nm for  
308 the 23 instruments was -2 % (range: -16 % to 7 %) before maintenance and -1 % (range: -14 % to 8 %) after  
309 maintenance, for soot measurements, emphasizing that the unit-to-unit variability was not significant. In our case,  
310 the post-processing of the datasets is the same for every site, therefore ensuring the comparability of the obtained  
311 concentration values. However, the main uncertainty in eBC concentrations lies in the various correction factors

312 applied and not in the raw measurement itself. Considering the various approaches commonly used to transform  
313 absorption coefficients into eBC mass concentrations, and related propagation of errors, an overall uncertainty of  
314 up to  $\pm 50\%$  can be associated with eBC estimates (Savadkoobi et al., 2024). Eventually, the Q-ACSM has been  
315 shown to display reproducibility uncertainties of 9 % on NR-PM<sub>1</sub> measurement, with uncertainties of 15, 19, 28,  
316 and 36 % for NO<sub>3</sub>, Org, SO<sub>4</sub>, and NH<sub>4</sub>, respectively (Crenn et al., 2015). The high uncertainties of SO<sub>4</sub> may be  
317 related to the RIE SO<sub>4</sub>, especially since it was considered constant in the early years. Additional uncertainties are  
318 related to possible measurement artifacts associated with interferences due to the nitrate (and sulfate) signal (e.g.,  
319 the Pieber effect on the CO<sub>2</sub><sup>+</sup> signal at m/z 44; Pieber et al., 2016). This artifact is explained by NO<sub>3</sub> (or SO<sub>4</sub>)  
320 induced reactions on the vaporizer and ionizer surfaces, producing CO<sub>2</sub> and therefore increasing the m/z 44 signal  
321 that is otherwise attributed to the organic aerosol. It can be quantified and evaluated over time by tracking the m/z  
322 44 / NO<sub>3</sub> (m/z 30 / SO<sub>4</sub>) ratios during the different calibrations performed with pure ammonium nitrate (ammonium  
323 sulfate) solutions. During the ACSM intercomparison at ACMCC in 2016 (Frenay et al., 2019), the m/z 44 / NO<sub>3</sub>  
324 ratio was determined to vary between 0.01 and 0.26 for 15 instruments, and the m/z 30 / SO<sub>4</sub> ratio between 0.01  
325 and 0.173. These were checked for each instrument in this study using calibration data and the results obtained fell  
326 within these ranges thus no correction was applied. The overestimation of PM<sub>1</sub> could also be linked to a change in  
327 the chemical composition of organic aerosols when this fraction dominates (e.g. Nault et al., 2023; Xu et al., 2018),  
328 since for organics the RIE is considered constant (1.4 by default) and these species are not considered in the  
329 Middlebrook correction (Middlebrook et al., 2012). Finally, other uncertainties can be related to size selection. It  
330 should be noted that the ACSM aerodynamic lens system is considered to be fully efficient for particles from 40  
331 nm up to 600 nm (Liu et al., 2007), while recent studies are suggesting collection size ranges that might be  
332 considered as instrument-specific (Poulain et al., 2020).

### 333 3 Phenomenology of fine aerosol chemistry in French urban environments

334 ~~accounts for the condensation of semivolatile organic compounds onto the organic and aqueous phases of particles~~  
335 ~~as well as the effect on partitioning of interactions between organic and inorganic compounds based on their~~  
336 ~~molecular structure. Thermodynamic equilibrium was assumed for gas-particle partitioning.~~

337 ~~The Secondary Organic Aerosol (SOA) mechanism of Wang et al., (2024) was used. This mechanism was obtained~~  
338 ~~by using the GENOA (GENERator of reduced Organic Aerosol) v2.0 algorithm (Wang et al., 2022, 2023) in order~~  
339 ~~to reduce the SOA mechanisms for monoterpenes and sesquiterpenes from the Master Chemical Mechanism~~  
340 ~~(Saunders et al., 2003) coupled with PRAM (in order to account for SOA formation from monoterpenes by auto-~~  
341 ~~oxidation) (Roldin et al., 2019). Following Wang, (2023), the hydrophilic/hydrophobic organics (Chrit et al., 2017)~~  
342 ~~mechanism was used for other precursors. Primary organic aerosols are treated as semivolatile organic compounds~~  
343 ~~that partition as a function of environmental conditions and can undergo ageing (Couvidat et Bessagnet 2021).~~

344 ~~Boundary conditions were taken from CAMS CIFS global model simulations (Flentje et al., 2021). Meteorological~~  
345 ~~data were obtained from the operational analysis of the Integrated Forecasting System (IFS) model of the European~~  
346 ~~Centre for Medium Range Weather Forecasts (ECMWF) (Flentje et al., 2021). Anthropogenic emissions of gases~~  
347 ~~and particles were taken from the CAMS REG-AP inventory (version v5.1\_REF2.1) (Kuenen et al., 2022).~~

a mis en forme : Espace Avant : 0 pt, Après : 8 pt

a mis en forme : Police : Non Italique

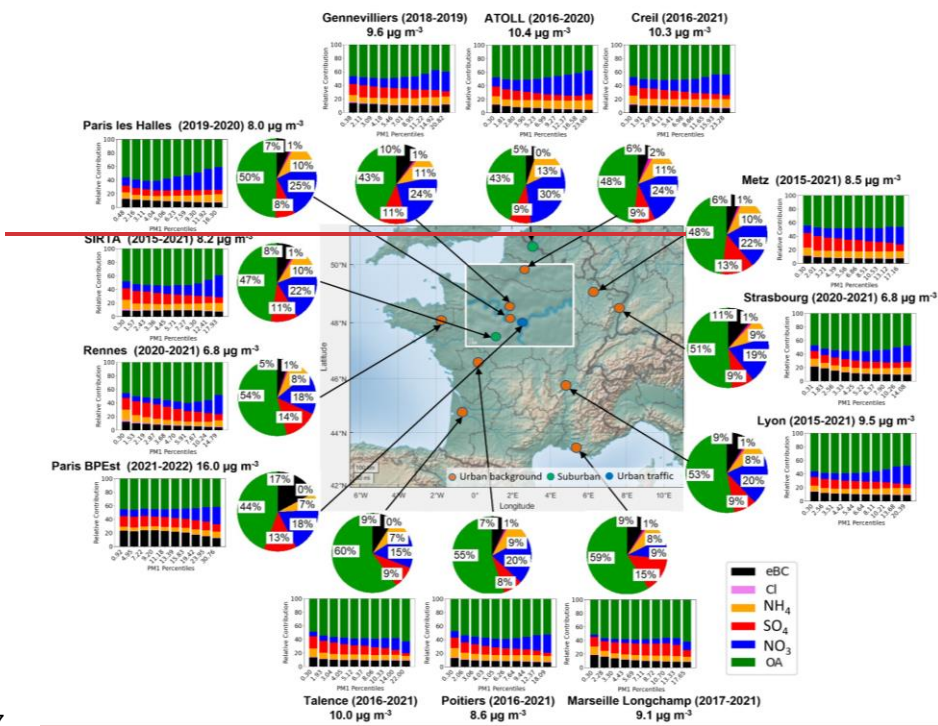
**349 3.1 Geographical specificities in the chemical composition**

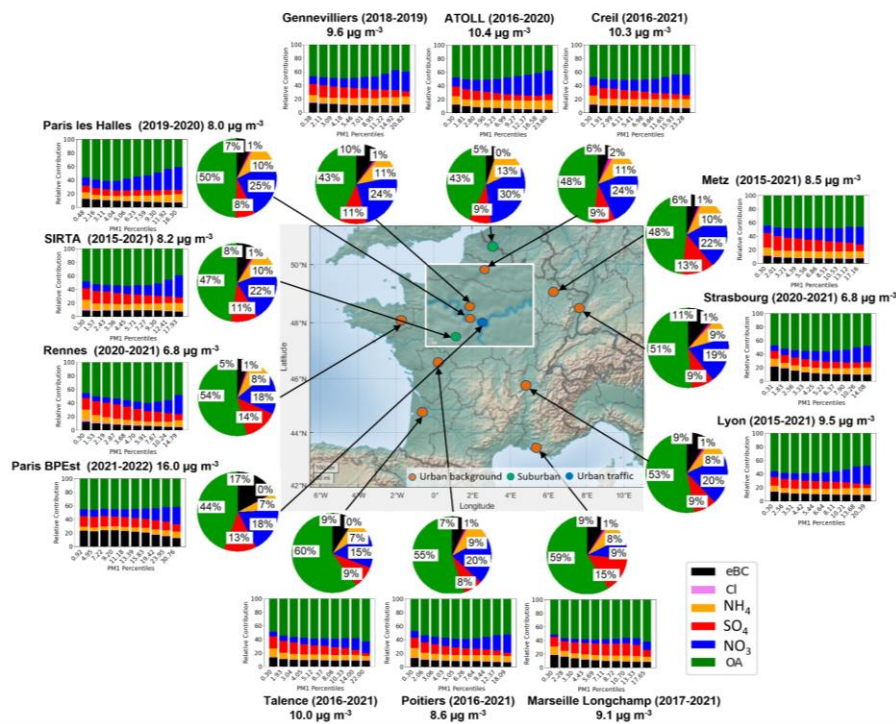
350 Figure 2 summarizes the PM<sub>1</sub> average values, as well as their relative contributions as pie charts and barplots,  
351 calculated according to the PM<sub>1</sub> percentiles at various sites in France.

352 The mean PM<sub>1</sub> concentrations at the 13 sites range from 6.8 to 16.0 µg m<sup>-3</sup>, reflecting the specificities of each  
353 urban site. These levels are comparable with the annual average NR-PM<sub>1</sub> levels reported by Bressi et al., (2021)  
354 across 21 sampling sites in Europe (from 2.8 to 14 µg m<sup>-3</sup>, including remote mountain sites), with the highest NR-  
355 PM<sub>1</sub> concentrations observed in mid-latitude Europe. In addition, Chen et al., (2022) reported an average PM<sub>1</sub>  
356 concentration of 12.2 ± 9.3 µg m<sup>-3</sup> for 13 urban sites in Europe. In the present study, PM<sub>1</sub> averaged 9.4 ± 8.3 µg  
357 m<sup>-3</sup> and PM<sub>2.5</sub> 11.5 ± 9.2 µg m<sup>-3</sup>. It is important to note that this multi-year PM<sub>2.5</sub> level exceeds the annual WHO  
358 guideline value of 5 µg m<sup>-3</sup> for PM<sub>2.5</sub> (WHO, 2021), as is the case at most sites in Europe (EEA, 2021).

359 Figure 3 further displays some key statistics on the various chemical species as well as for PM<sub>1</sub> and PM<sub>2.5</sub> mass  
360 concentrations, as a function of mean levels measured at each site. The only site with a “Road-Traffic” typology  
361 (BPEst), located on the east side of the Paris ring road, exhibits the highest mean PM<sub>1</sub> concentration (16.0 µg m<sup>-3</sup>,  
362 standing out notably on eBC, SO<sub>4</sub>, and OA levels (Fig. 3). On the other hand, Rennes and Strasbourg display  
363 the lowest mass concentrations of PM<sub>1</sub> (6.8 µg m<sup>-3</sup>), both having the lowest levels of OA (around 3.5 µg m<sup>-3</sup>). In  
364 addition, the site in Rennes shows a significantly lower mean eBC level (0.4 µg m<sup>-3</sup>), compared to the general  
365 average (0.8 µg m<sup>-3</sup>), thus depicting a lower influence of combustion aerosols at this site. The remaining sites  
366 generally exhibit a fairly homogeneous PM<sub>1</sub> mass concentration, ranging from about 8 to 10 µg m<sup>-3</sup>. ATOLL, Creil  
367 and Talence sites have higher PM<sub>1</sub> concentrations (between 10 and 10.4 µg m<sup>-3</sup>): the first two (located in the  
368 northern Hauts-de-France region) are influenced by higher NO<sub>3</sub> concentration levels of 3.1 and 2.4 µg m<sup>-3</sup>,  
369 respectively, whereas Talence (near Bordeaux in the southern Nouvelle-Aquitaine region) has a strong contribution  
370 of OA (6.0 µg m<sup>-3</sup>).

371 The high NO<sub>3</sub> levels at the two sites in northern France are attributed to road traffic and combustion emissions  
372 (rich in nitrogen oxides; NO<sub>x</sub>), which combine with ammonia (NH<sub>3</sub>), typically associated with agricultural  
373 activities, forming ammonium nitrate (NH<sub>4</sub>NO<sub>3</sub>; AN) under favorable meteorological conditions (Roig Rodelas et  
374 al., 2019), as well as to transboundary pollution from Eastern Europe (Chebaicheb et al., 2023). Conversely,  
375 Talence has the highest 95<sup>th</sup> percentile of OA (higher than 19.0 µg m<sup>-3</sup>, Fig. 3), associated with strong biomass  
376 combustion in the Bordeaux area during the cold season (Favez et al., 2021).

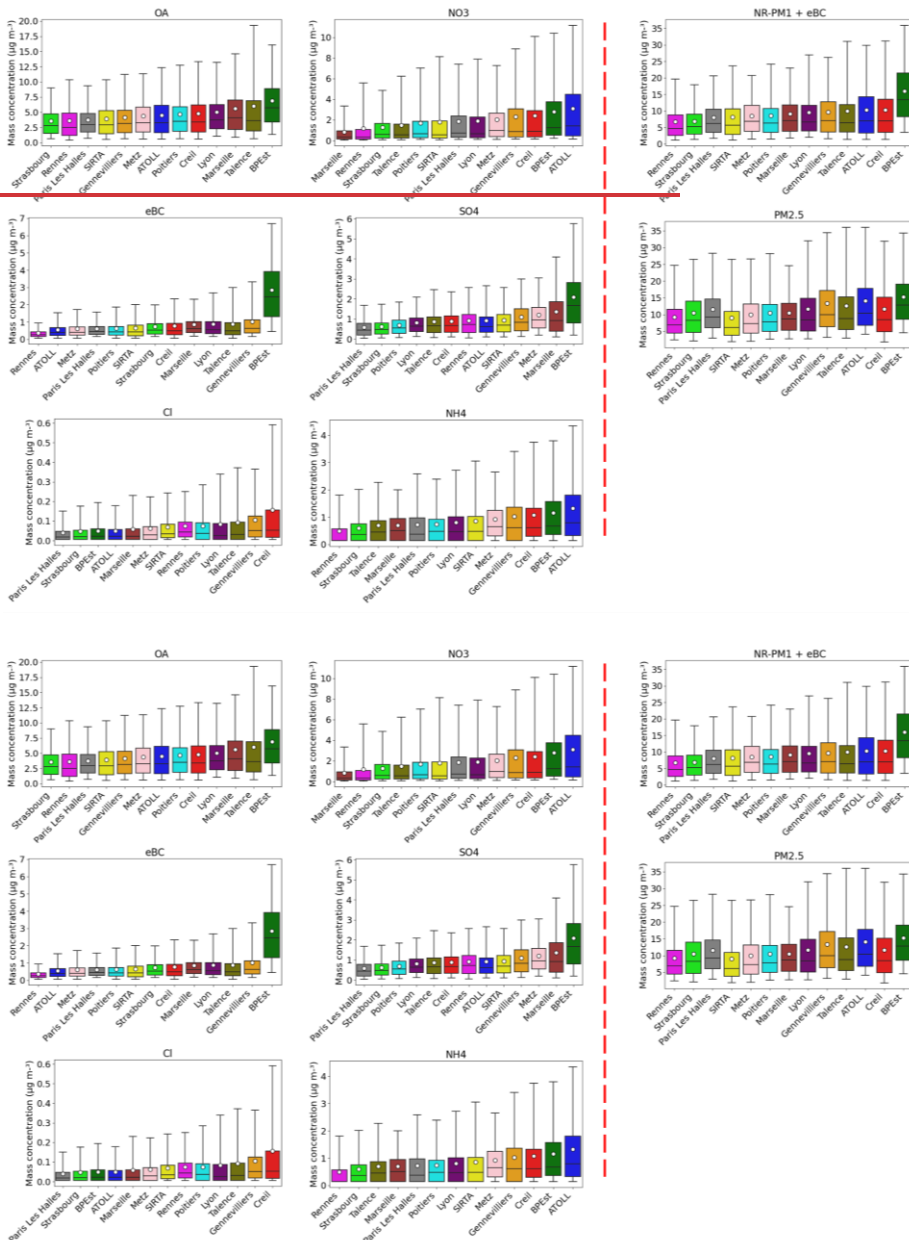




378

379 **Figure 2: Multi-annual averaged PM<sub>1</sub> mass concentration and pie charts of average relative contributions of non-**  
 380 **refractory species and eBC at different sites in France; the bar charts represent the relative contribution**  
 381 **of PM<sub>1</sub> deciles.**

382  
 383 For the Greater Paris region, the Sirta facility is located 22 and 25 km away from the sites representing central  
 384 areas of Paris, i.e., Paris Les Halles and Gennevilliers, respectively. Logically, due to the closer proximity with  
 385 intense emission sources, Gennevilliers exhibits higher PM<sub>1</sub> concentrations ( $9.6 \mu\text{g m}^{-3}$  on average over the 2018-  
 386 2019 period) compared to Sirta levels of  $8.2 \mu\text{g m}^{-3}$ . The comparable PM<sub>1</sub> loading presented here between Paris  
 387 Les Halles ( $8.0 \mu\text{g m}^{-3}$ ) and Sirta is probably linked to the specific measurement periods analyzed for each site.  
 388 Indeed, data from Paris Les Halles presented here include the COVID-19 lockdown periods of 2020-2021, while  
 389 Sirta data are averaged over 2015-2021. When averaged over the same period as Paris Les Halles, the PM<sub>1</sub> level  
 390 at Sirta decreases to  $6.2 \mu\text{g m}^{-3}$ . Moreover, an increased mixing layer height over the Paris city center, due to  
 391 the urban heat island effect which may dilute the aerosol content in a wider volume during daytime, should also  
 392 be considered when comparing concentrations from inner and suburban sites within such a megapolis (e.g., Dupont  
 393 et al., 2016).



394

395

396

397

Figure 3: Box plots of the statistical distribution (5<sup>th</sup>, 25<sup>th</sup>, 50<sup>th</sup>, 75<sup>th</sup> and 95<sup>th</sup> percentiles) of each NR-PM<sub>1</sub> species and eBC, as well as PM<sub>1</sub> and PM<sub>2.5</sub> mass concentrations; means are indicated by the circle symbol.

398

399 The analysis of individual contributions shows that organic compounds make up about half of the PM<sub>1</sub> total mass  
400 across all sites, ranging from 43 to 60 %, which is comparable with the average of OA at urban sites in Europe  
401 (around 50 % of PM<sub>1</sub>), as reported by Chen et al., (2022). It is also consistent with the OA relative contribution  
402 observed by Bressi et al., (2021) in Europe (36-64 % of NR-PM<sub>1</sub>). The stations located in central and southern  
403 France, including Marseille-Longchamp, Poitiers, Talence, and Lyon, show higher OA mass concentrations than  
404 sites in the north, which can be partly due to more intense secondary formation. Conversely, NO<sub>3</sub> contributions  
405 are more pronounced at northern sites (22-30 % vs 9-20 % at southern sites), due to more favorable  
406 conditions for particulate AN formation (e.g., Favez et al., 2007). Consequently, NO<sub>3</sub> mass concentrations in  
407 France decreased from north to south and from east to west, consistent with the findings by Favez et al., (2021).  
408 Furthermore, NO<sub>3</sub> constitutes the second most significant contributor, accounting for 15-30 % of PM<sub>1</sub> mass, except  
409 for Marseille-Longchamp, where it is less than 10 % (0.8 µg m<sup>-3</sup>). Other studies have also reported the  
410 predominance of NO<sub>3</sub> over SO<sub>4</sub> at many European sites (Bressi et al. 2021, Chen et al. 2022). As Marseille is  
411 characterized by high emissions from industry and shipping activities, the Marseille-Longchamp site exhibits a  
412 higher contribution of SO<sub>4</sub> (15 %), making it the second major contributor to PM<sub>1</sub> at that site (Chazeau et al.,  
413 2021).

414 Overall, SO<sub>4</sub> is the third largest contributor in France, with contributions ranging from 8 to 14 %. Besides  
415 Marseille-Longchamp and the BPEst traffic site, significant SO<sub>4</sub> concentrations are also obtained for Metz and  
416 Gennevilliers (around 1 µg m<sup>-3</sup> on average), probably reflecting their transport from SO<sub>2</sub>-rich regions, given that  
417 local emissions are considered low or negligible. Furthermore, SO<sub>4</sub> is considered to be influenced by long-range  
418 transport from Central Europe, which is the case for many sites in northern and Eastern France, including SIRTA,  
419 ATOLL, Creil, Paris Les Halles, Strasbourg, and Poitiers.

420 For the remaining compounds, mean NH<sub>4</sub> levels range from 0.5 to 1.3 µg m<sup>-3</sup>, with a contribution fluctuating  
421 between 7 % and 13 %, showing a strong correlation with NO<sub>3</sub> and SO<sub>4</sub> levels, linked to the neutralization of  
422 sulfuric and nitric acids by NH<sub>3</sub>. Meanwhile, the contribution of eBC varies from 5 to 11 % at the urban background  
423 sites investigated here. Previous studies, including Chen et al. (2022), reported higher contributions of BC at  
424 different European urban sites (12 %), which can be explained by recent changes in data processing, as discussed  
425 in Section 2.3.2. Finally, Cl makes a minor contribution of around 1 % at all sites, with averaged mass  
426 concentrations generally very low, remaining below 0.1 µg m<sup>-3</sup>, except for Gennevilliers (0.1 µg m<sup>-3</sup>) and Creil  
427 (0.15 µg m<sup>-3</sup>), with a slightly higher contribution of 2 %. Ammonium chloride (AC; NH<sub>4</sub>Cl) is formed in the  
428 atmosphere from the chemical reaction of hydrochloric acid (HCl) and NH<sub>3</sub>. The main sources of HCl in the  
429 atmosphere are biomass combustion (Andreae et al., 1996), coal burning (Tobler et al., 2020, 2021), and waste  
430 combustion (McCulloch et al., 1999). In Creil, there is a large waste treatment plant 2 km northeast of the  
431 monitoring station, which could explain the higher concentration of Cl observed at this site (Fig. S3). Similarly, in  
432 Gennevilliers, industrial emissions could explain occasional spikes measured during easterly winds.

433 Figure 2 also illustrates the variations in PM<sub>1</sub> chemical composition as a function of PM<sub>1</sub> mass concentrations,  
434 divided into 10 concentration levels (corresponding to deciles) for each site. OA exhibits even higher contributions  
435 at high PM<sub>1</sub> mass concentrations at Talence, Marseille-Longchamp, and Poitiers especially during the coldest and  
436 warmest months of the year (Figure S4). This can generally be explained by the influence of biomass burning  
437 during winter pollution episodes as also previously described for the Paris area (Petit et al., 2015; Foret et al.,



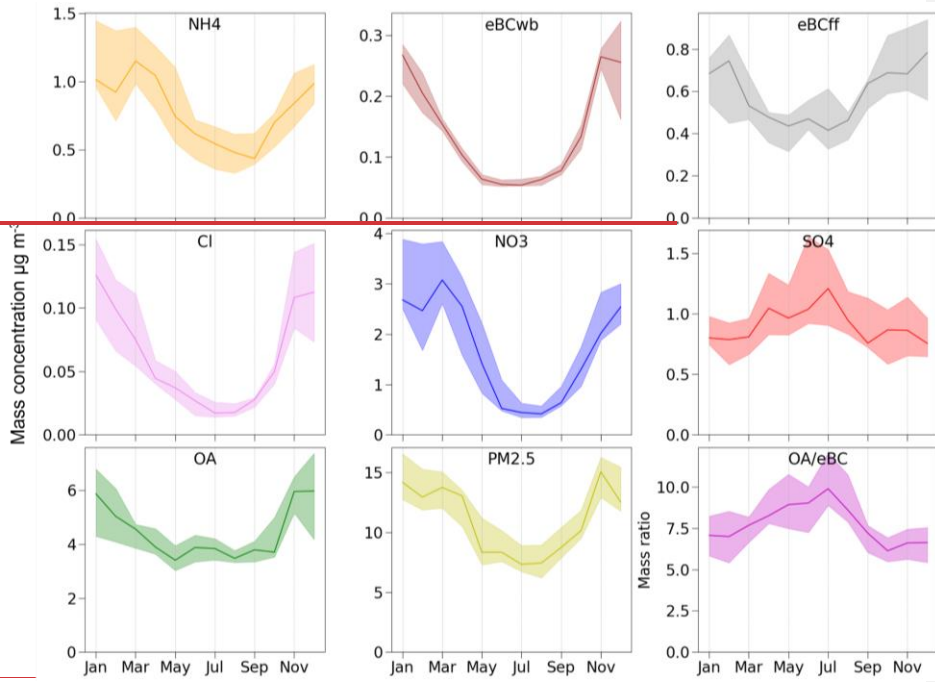
438 2022), and by the impact of secondary formation of organic compounds and emissions from forest fires in summer  
439 (Chen et al., 2022). However, OA decreases from the 30<sup>th</sup> percentile (around 4 to 5  $\mu\text{g m}^{-3}$ ) of  $\text{PM}_{10}$  levels with an  
440 increase in  $\text{NO}_3$  at sites in northern France and Lyon.  $\text{NO}_3$  plays an important role during pollution events,  
441 particularly in spring, as reported previously in France (Dupont et al., 2016; Petit et al., 2017; Zhang et al., 2020)  
442 and at other mid-latitude European sites (Bressi et al., 2021).

443 The contributions of  $\text{SO}_4$  and eBC are generally stable or show a slight decrease with increasing  $\text{PM}_{10}$ . Nevertheless,  
444 eBC exhibits significant contributions at lower  $\text{PM}_{10}$  levels at BPEst and, to a lesser extent, Marseille-Longchamp,  
445 Strasbourg, and Rennes, indicating significant local combustion sources at those sites. Furthermore, Marseille-  
446 Longchamp exhibits fairly consistent OA,  $\text{NO}_3$ , and  $\text{SO}_4$  contributions to  $\text{PM}_{10}$  levels, showing nonetheless a  
447 significant increase of the first two during pollution events. Globally,  $\text{SO}_4$  is a relevant contributor for Metz,  
448 Rennes, Gennevilliers, SIRTa, Talence, and Marseille-Longchamp, while OA retains significance at all sites  
449 throughout the  $\text{PM}_{10}$  percentiles.

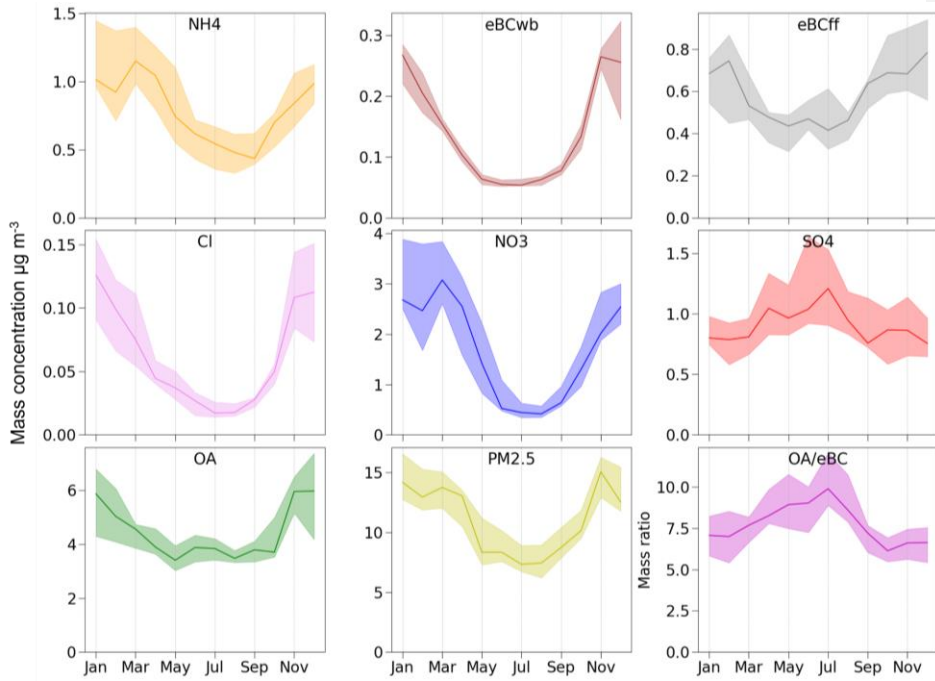
### 450 3.2 Seasonal and diel cycles of fine aerosol chemical species

451 The averaged seasonal and diel cycles were investigated for the different chemical species at all sites. Figure 4  
452 shows the median and interquartile range (IQR) monthly variability for each species considered here, over the  
453 averaged cycles for the (sub)urban sites over France. The averaged monthly variabilities of the  $\text{PM}_{10}$  species for  
454 each site are shown in Figure S5.

455 All chemical species exhibit significant variability in mass concentration over the months. In particular,  $\text{eBC}_{\text{wb}}$   
456 shows a clear seasonality, with higher concentrations during winter (around an average of 0.3  $\mu\text{g m}^{-3}$ ) compared  
457 to summer (0.05  $\mu\text{g m}^{-3}$ ), as expected due to the high level of wood combustion for residential heating in  
458 wintertime. Furthermore, there is substantial variability between sites in winter (represented by a larger IQR),  
459 probably as a result of different meteorological conditions, as well as the fraction of wood combustion for  
460 residential heating in the surroundings. Conversely,  $\text{eBC}_{\text{ff}}$  shows seasonal variations comparable to  $\text{eBC}_{\text{wb}}$ , but  
461 with smaller winter/summer difference spans ranging from around 0.4 to 0.7  $\mu\text{g m}^{-3}$  in May and October,  
462 respectively. This variability is associated with seasonal meteorological conditions favoring (or not) the  
463 accumulation of atmospheric pollutants, compounded to a lesser extent to changes in road traffic intensity, leading  
464 to a maximum commonly observed in autumn (Petit et al., 2015). Similarly, OA displays higher levels during cold  
465 seasons (5.5  $\mu\text{g m}^{-3}$ ), with reasons comparable to those for eBC, and lower levels during warm periods (3.5  $\mu\text{g m}^{-3}$ ).  
466 Nevertheless, OA peaks (with a higher OA/eBC mass ratio) in summer, reflecting the formation of  
467 SOAsecondary organic aerosol (SOA) from biogenic and anthropogenic sources (Favez et al., 2007). Notably,  
468 SOAs are formed mainly from biogenic VOC in summer, when temperatures and sunlight are high (Canonaco et  
469 al., 2015; Cao et al., 2022), but also during nighttime, likely associated with nitrate chemistry (Kiendler-Scharr  
470 et al., 2016). Furthermore, OA yields lower site-to-site variability (i.e., IQR) (Fig. S6), as most of the OA, even in  
471 wintertime, is associated with regional processes and secondary formation (Chen et al., 2022; Chebaicheb et al.,  
472 2023).



473



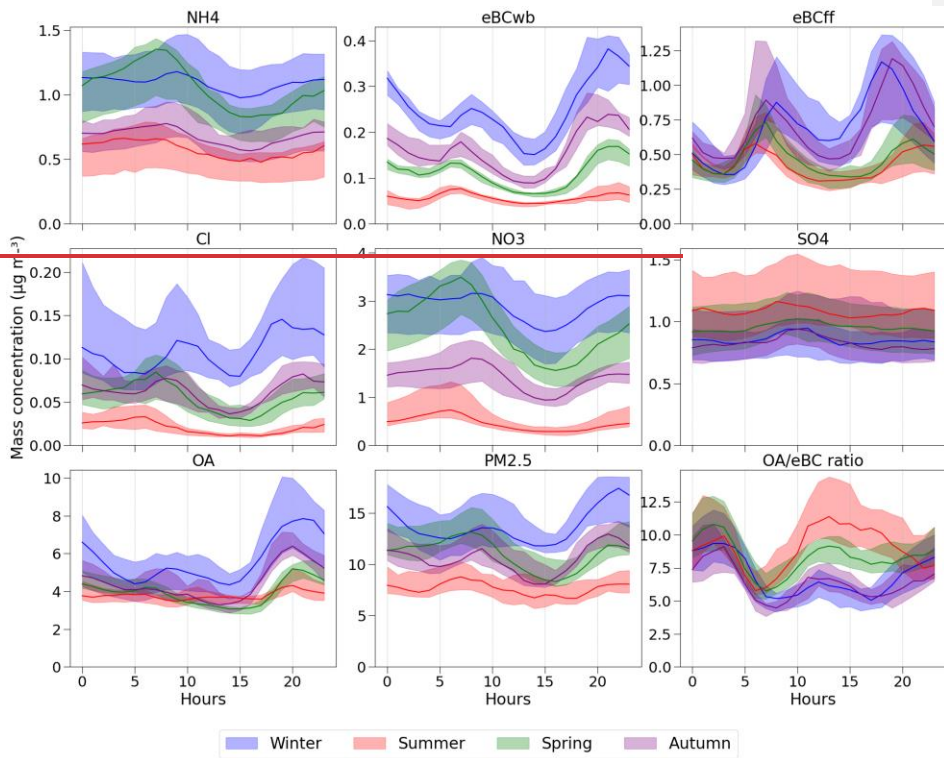
474

475 **Figure 4: Monthly variability of mass concentrations of PM<sub>1</sub> species, PM<sub>2.5</sub>, and OA/eBC ratio across all sites. The**  
476 **Figure shows the median and IQR (25<sup>th</sup> and 75<sup>th</sup> percentiles) calculated from the averaged monthly concentrations for**  
477 **each site. Months were considered only if data coverage was at least 75 %.**

478

479 NO<sub>3</sub> and NH<sub>4</sub> concentrations display a marked seasonal pattern, peaking in late winter and early spring, and  
480 averaging around 3.0 and 1.2 μg m<sup>-3</sup>, respectively. As discussed in the previous section, AN concentrations depend  
481 on site-specific factors, contributing to a greater variability between sites. In contrast, SO<sub>4</sub> shows a relatively stable  
482 monthly variation, with higher levels observed between April and August. Elevated summertime SO<sub>4</sub>  
483 concentrations could be attributed to favorable meteorological conditions. In addition, SO<sub>4</sub> can either be formed  
484 “locally” from the oxidation of SO<sub>2</sub> or transported from emission hotspots, such as Eastern European regions (Roig  
485 Rodelas et al., 2019). Cl exhibits a strong seasonality, ranging from 0.02 (summer) to 0.14 μg m<sup>-3</sup> (winter). The  
486 higher concentrations of HCl during the cold seasons can be partly attributed to its semi-volatile nature (similarly  
487 to AN, its formation should be favored by low temperatures and high humidity), as well as transport from emission  
488 hotspots areas, notably of intense coal combustion, further enhanced during wintertime (Tobler et al., 2021).

489 The mean diel profiles obtained for each chemical species across all (sub)urban background sites and for each  
490 season are shown in Figure 5. All species exhibit higher concentrations at night, which could be, at least partially,  
491 associated with a lower boundary layer height. Some species show variability associated with local emission  
492 sources, including road traffic (morning and evening peaks), notably for OA and eBC<sub>ff</sub>, with consistent behavior  
493 throughout the year. OA shows a stronger nighttime peak, notably during the colder months, mimicking eBC<sub>wb</sub>  
494 associated with wood heating. OA enhancement during nighttime in wintertime is linked with residential heating  
495 under a lower boundary layer (ChebaichebFavez et al., [in-prep.,2021](#)). Furthermore, at Paris Les Halles, in the  
496 heart of the city center, OA further exhibits a small peak at noon (Fig. S7), pointing to a possible influence of  
497 cooking emissions at this site. Overall, the PM<sub>2.5</sub> profile aligns with OA diel cycles, with higher loadings during  
498 the morning and evening hours, due to the predominance of the organic species in the fine aerosol fraction.



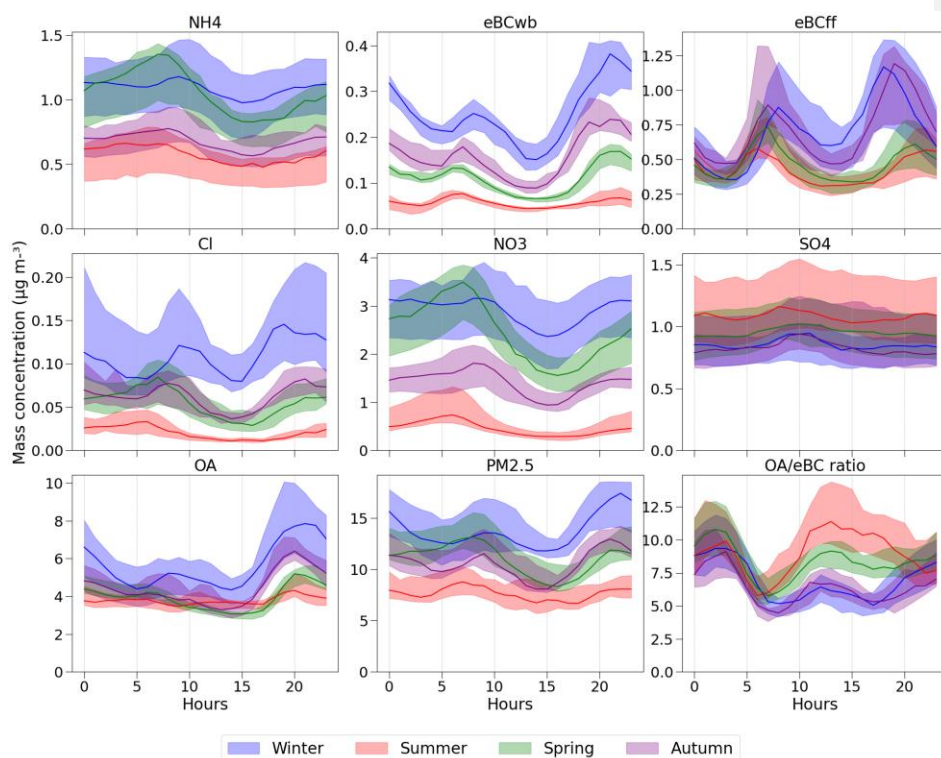


Figure 5: Seasonal median and IQR of daily profiles for all sites for each  $PM_{10}$  component,  $PM_{2.5}$ , and OA/eBC ratio.

Both  $NO_3$  and  $NH_4$  display a comparable diel cycle, featuring higher mass concentrations during the morning hours in all seasons, albeit at different levels. Lower temperatures and higher relative humidity in the morning favor the formation of AN. During the day, as temperatures rise, AN concentrations decrease due to the evaporation into the gas phase of  $NH_3$  and  $HNO_3$ . Consequently, AN mass concentrations are lowest in summer, due to unfavorable weather conditions and, to some extent, reduced  $NO_x$  levels associated with the school holidays (Roig Rodelas et al., 2019). As discussed previously, AN levels are highest in spring, due to favorable meteorological conditions and intensive agricultural activities. On the other hand, the diel cycle of  $SO_4$  shows relatively constant values during the day, with higher levels observed in summer, as discussed previously. Notably, the diel cycle of  $SO_4$  at some sites features morning or afternoon peaks, especially for Lyon and Marseille-Longchamp sites, which may be explained by the presence of local (Chazeau et al., 2021) or regional sources (Fig. S7, S8, and S9).

Finally, the OA/eBC ratio shows an interesting diel cycle, exhibiting greater values at night in all seasons, ranging from 8 to 12, possibly associated with nighttime SOA formation or OA-rich sources such as wood combustion. This ratio also increases during the day, which could be explained by photochemistry and SOA formation, particularly of biogenic origin during summertime (Chebaicheb et al., 2023). As expected, the ratio decreases during the morning and evening rush hours, associated with more BC-rich traffic emissions.

517 **3.3 Examples of comparison – 4 Comparison between our observations and the CHIMERE Chemical**  
518 **Transport Model**

519 **Measurements of PM chemical transport composition are a valuable tool for validating atmospheric CTMs,**  
520 **particularly for assessing their accuracy and reliability. In particular, observations and model outputs**

521 In this section, CHIMERE- are complementary to track complex atmospheric sources and processes, including  
522 chemical transformations leading to secondary PM formation. Comparing chemically-speciated observations with  
523 CTM model results enables discrepancies to be identified and could provide clues on model improvement. In  
524 addition, near-real-time observations allow gauging a model ability to represent the temporal and spatial  
525 distributions of atmospheric pollutants, which is essential for forecasting air quality and assessing environmental  
526 policies and scenarios. The continuous observations provided by the CARA program are of great importance for  
527 the continuous improvement of 3D air quality models, notably CHIMERE, leading to more accurate forecasts and  
528 a better understanding of atmospheric processes.

529 **4.1 Model description**

530 In order to exemplify the comparison of our database with CTM's outputs, 3D simulations were performed with  
531 the CHIMERE version of Wang et al. (2024) which is based on a coupling between CHIMERE (Menuet et al.,  
532 2021) and SSH-aerosol v1.3 aerosol model (Sartelet et al., 2020). The Secondary Organic Aerosol (SOA)  
533 mechanism of Wang et al. (2024) was used. This mechanism was obtained by using the GENOA (GENerator of  
534 reduced Organic Aerosol) v2.0 algorithm (Wang et al., 2022, 2023) to reduce the SOA mechanisms for  
535 monoterpenes and sesquiterpenes from the Master Chemical Mechanism (Saunders et al., 2003) coupled with  
536 PRAM (accounting for SOA formation from monoterpenes by auto-oxidation) (Roldin et al., 2019). Following  
537 Wang (2023), the hydrophilic/hydrophobic organics (Chrit et al., 2017) mechanism was used for other precursors.  
538 Primary organic aerosols are treated as semivolatile organic compounds that partition as a function of  
539 environmental conditions and can undergo ageing (Couvidat and Bessagnet 2021).

540 One important feature of SSH-aerosol consists in the computation of gas-particle partitioning with the  
541 thermodynamic module ISORROPIA (Nenes et al., 1998) and SOAP (Secondary Organic Aerosol Processor,  
542 Couvidat and Sartelet, 2015) models for inorganic and organic aerosols, respectively. The latter accounts for the  
543 condensation of semivolatile organic compounds onto the organic and aqueous phases of particles as well as the  
544 effect on partitioning of interactions between organic and inorganic compounds based on their molecular structure.  
545 Thermodynamic equilibrium was assumed for gas-particle partitioning.

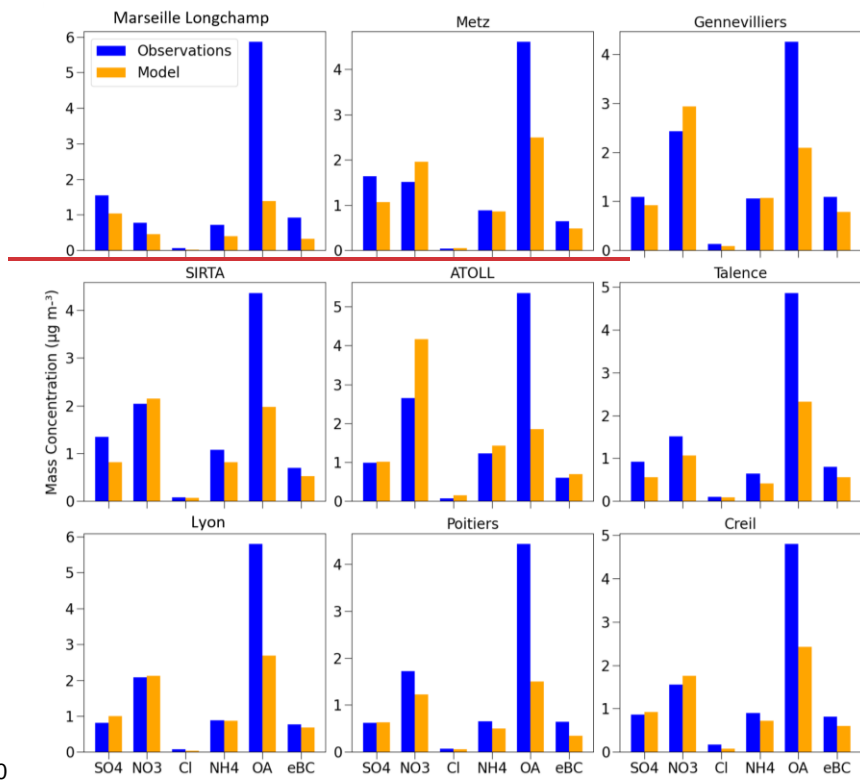
546 Meteorological data were obtained from the operational analysis of the Integrated Forecasting System (IFS) model  
547 of the European Centre for Medium-Range Weather Forecasts (ECMWF) (Flentje et al., 2021). Boundary  
548 conditions were taken from CAMS CIFS (IFS coupled to a tropospheric chemistry scheme) global model  
549 simulations (Flentje et al., 2021) for chemical species. Anthropogenic emissions of gases and particles were taken  
550 from the CAMS-REG-AP inventory at a 0.05°x0.1° grid resolution (version v5.1 REF2.1) (Kuenen et al., 2022).

a mis en forme : Police :Non Italique

a mis en forme : Espace Avant : 0 pt, Après : 8 pt

551 **4.2 Comparison results**

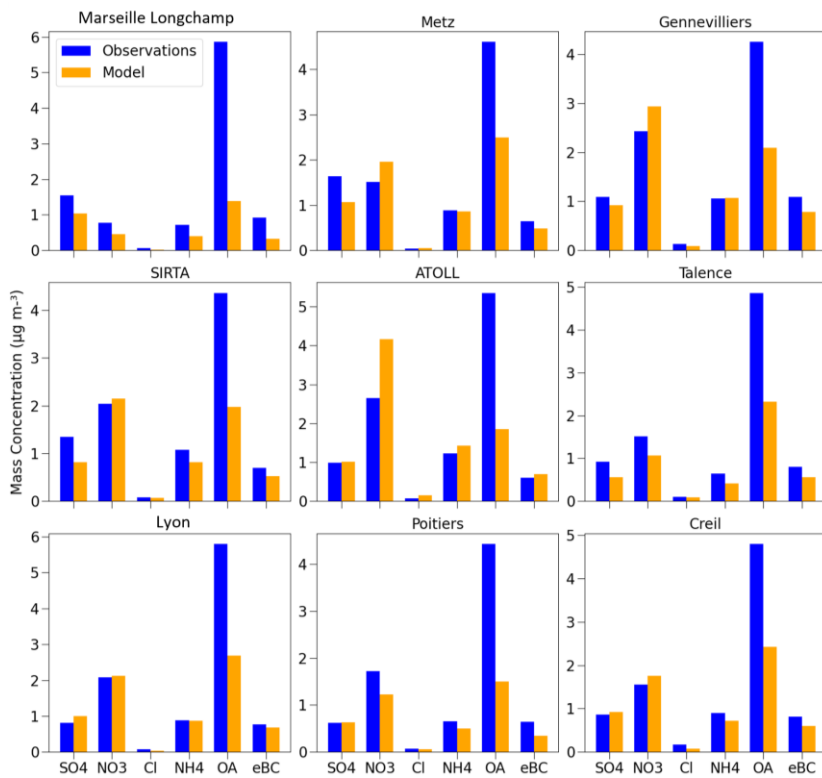
552 CHIMERE model results for the year 2018, with a spatial resolution of 7 km over France, were used to compare  
553 with PM<sub>1</sub> observations. ~~The simulation results could only be compared with 9 at nine~~ of the sites analyzed  
554 ~~here where data were available (excluding BPEst, Paris Les Halles, Rennes, and Strasbourg were excluded from~~  
555 ~~this analysis because measurements at these sites only started after 2018.)~~. The time series of observed and modeled  
556 concentrations are shown in the supporting material (Figure S10). Figure 6 summarizes results from the  
557 comparison between observations and simulations, typically showing good agreement. Loadings for inorganics  
558 (NO<sub>3</sub>, SO<sub>4</sub>, NH<sub>4</sub>, and Cl) and eBC are fairly well captured by the model across all sites, with some exceptions. In  
559 particular, at the Marseille-Longchamp site, SO<sub>4</sub>, NO<sub>3</sub>, NH<sub>4</sub>, and eBC are consistently underestimated by the model  
560 (33, 41, 45, and 65 %, respectively). This discrepancy could be due to the low resolution of the model grid (~~7 km~~  
561 ~~over France)0.0625° x 0.125°) that may not be sufficient to capture local meteorology or sources, or more broadly~~  
562 a potential underestimation of emissions in the Southeastern region of France. Several sites also present an  
563 underestimation of SO<sub>4</sub> (Metz, SIRTa, Talence) by around 35-39 %. In contrast, NO<sub>3</sub> is strongly overestimated  
564 by the model (57 %) in the north of France (ATOLL). Organics, on the other hand, are consistently underestimated  
565 by the model at all sites by a factor of 2-3. Since eBC is well represented as discussed above, this leads to low  
566 modeled OA/eBC ratios (2.7-5.2, vs 3.9-8.8 for observed OA/eBC ratios), suggesting an underestimation of  
567 secondary organic aerosols in the model. Other recent studies also reported underestimations of OA at 11 European  
568 sites, focusing on winter 2009 (Ciarelli et al., 2016). In the present study, OA yields a strong underestimation  
569 particularly in the warmer months (60 % vs. 41 % for the colder months).



570

571



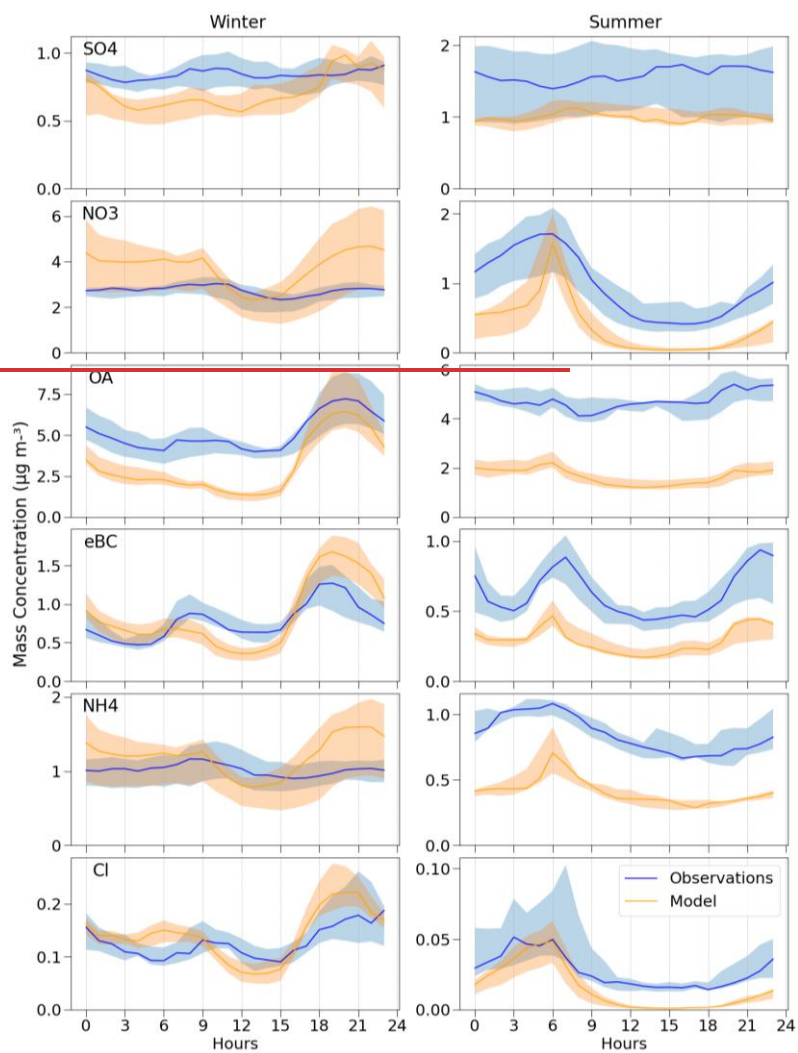


572  
 573 **Figure 6: Mean mass concentration (in  $\mu\text{g m}^{-3}$ ) of different chemical species for observations (in blue) and simulations**  
 574 **(in orange) at nine French sites over the year 2018.**

575 Figure 7 displays the diel profiles of each species, comparable with Figure 5, ~~however restricted to~~for the winter  
 576 and summer of 2018, ~~allowing (spring and autumn profiles can be found in the comparison with model outputs: SI,~~  
 577 ~~Figure S11).~~ In general, the species exhibit relatively consistent model performance between winter and summer,  
 578 although there is an underestimation by the model for the latter. For  $\text{NO}_3$ , the concentrations observed during  
 579 wintertime are relatively stable throughout the day, whereas the model shows a strong daytime decrease due to the  
 580 modeled ~~evaporation/volatilization~~ of ammonium nitrate. During summertime, ~~an~~ enhancement of  $\text{NO}_3$  in the early  
 581 morning is captured by both observations and model, however as a smooth nighttime increase/decrease for the  
 582 former, and a sharp peak in the latter. A similar pattern is observed for  $\text{NH}_4$ . For  $\text{SO}_4$ , the diel profile is quite  
 583 constant for both observations and simulations in summer. In winter, the slight increase of  $\text{SO}_4$  during the day is  
 584 not captured by the model, which instead shows a low peak at night. For eBC, both observations and model  
 585 simulations show two peaks during rush hours. In winter, the night peak is more pronounced in the model, but  
 586 nonetheless they display comparable levels, in contrast to summertime, when the model tends to underestimate the  
 587 concentrations. These differences in daily eBC profiles may be attributed to meteorological conditions or issues in  
 588 the seasonal temporality of emissions. Finally for OA, as discussed ~~before~~above, the model largely underestimates

589 observations in summer. Generally, the behavior is fairly well represented, however the wintertime nighttime  
590 enhancement is larger than observations, similar to eBC.

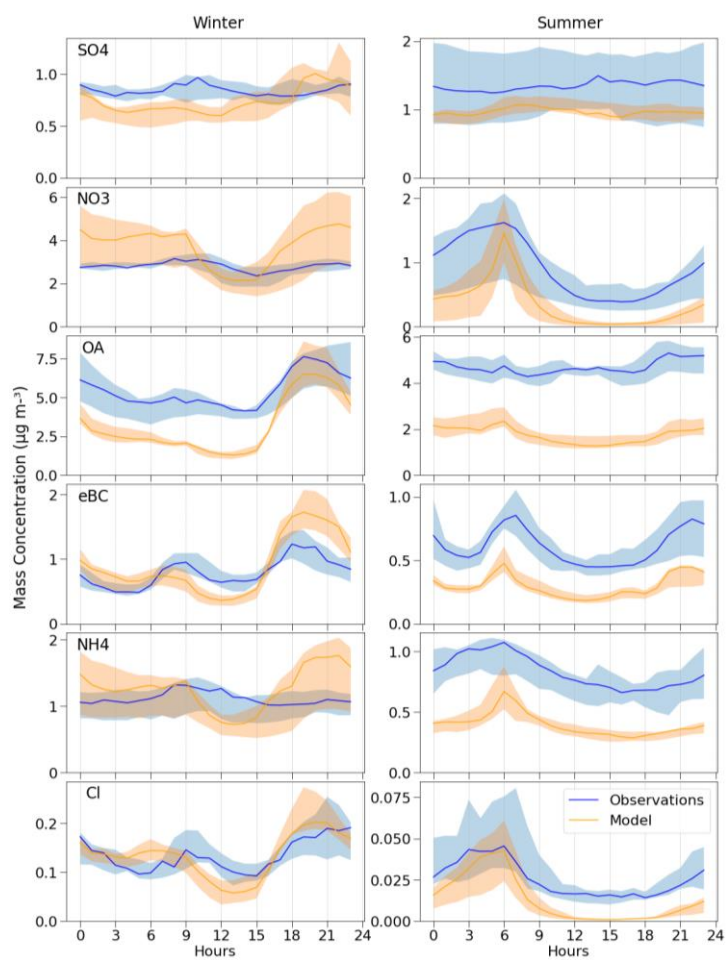
591 Figure 8 presents some statistical parameters (mean bias, normalized *Root Mean Square Error* (RMSE), and  
592 correlation coefficient  $r$ ) calculated from the daily means for each chemical species across the nine urban sites in  
593 France. Overall, the correlations between observations and model results show good agreement, with correlation  
594 coefficients ( $r$ ) ranging between 0.6 and 0.8, which is consistent with the literature (Couvidat et al., 2018,  
595 Cholakian et al. 2018). The mean bias and normalized RMSE confirm the model robustness. Mean bias is nearly  
596 negligible for  $\text{SO}_4$ ,  $\text{NO}_3$ ,  $\text{NH}_4$ , Cl, and eBC, and approximately  $-2 \mu\text{g m}^{-3}$  for OA, up to  $-4 \mu\text{g m}^{-3}$  for the Marseille  
597 Longchamp site. RMSE exhibits a slightly more scattered distribution, generally ranging between 0.5 and  $2 \mu\text{g m}^{-3}$ .  
598



599  
600 These comparisons between PM<sub>1</sub> observations and model simulations reveal underestimations or overestimations  
601 by the model for each species. However, it remains challenging to pinpoint the exact reasons for these  
602 discrepancies, though hypotheses can be made. Generally, there is good agreement for SO<sub>4</sub>. On the other hand,  
603 significant peaks of modeled NO<sub>3</sub> and NH<sub>4</sub> are observed, particularly in November and December at northern  
604 France stations, which may be explained by an overestimation of NH<sub>3</sub> emissions during this period in the model  
605 (Couvidat et al., 2018). For eBC, the results vary from one station to another, which may be linked to issues with  
606 the spatial distribution of emissions, which are not sufficiently accurate. OA is consistently underestimated across  
607 all stations. Further speciation of OA could provide more insights in this regard, which will be discussed in a

608 [forthcoming article on OA sources. Ultimately, conducting further simulations over other periods could help](#)  
609 [improve the model.](#)

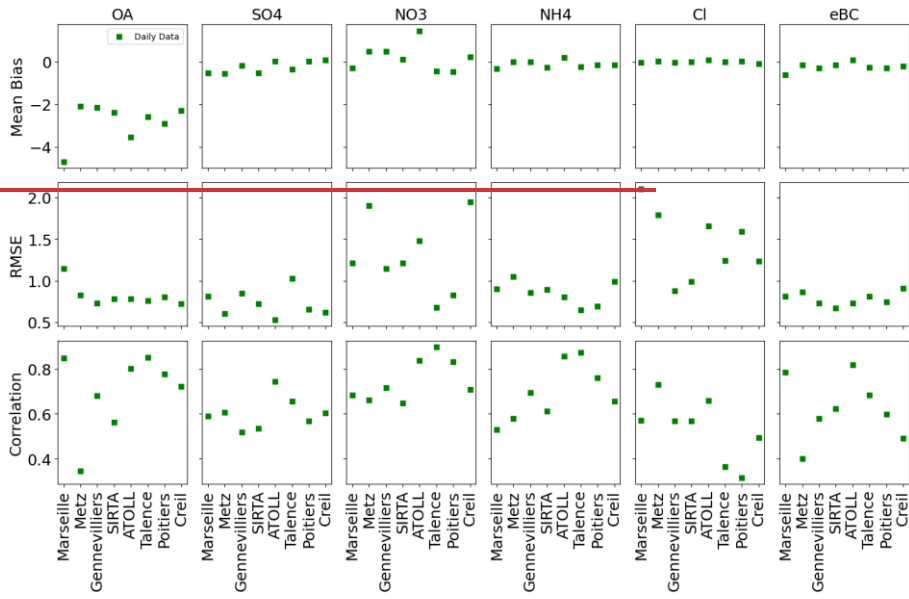
610



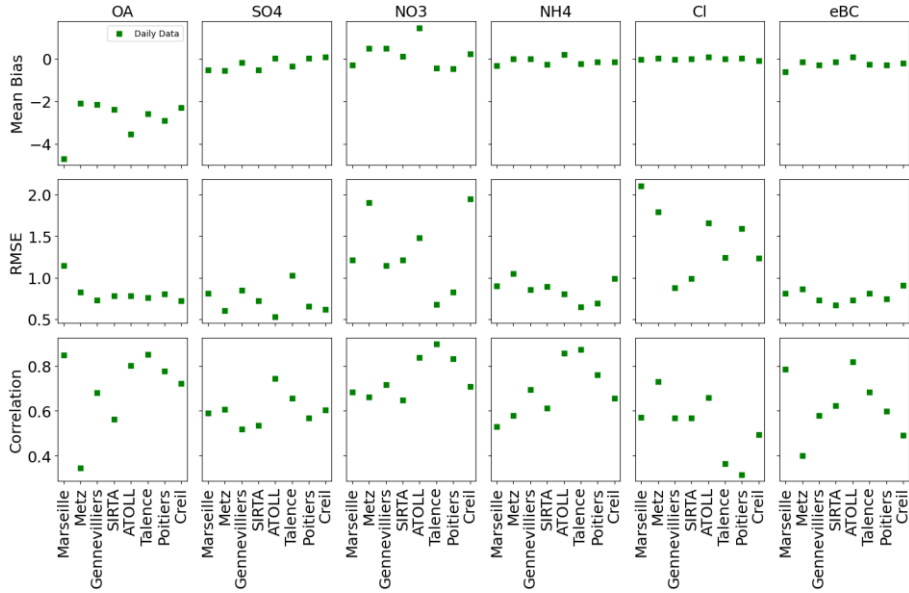
611

612 **Figure 7: Observed and modeled diel profiles during the winter and summer of 2018 across 9 French sites.**

613



614



615 **Figure 8: Statistic parameters (mean bias, normalized RMSE, and correlation coefficient  $r$ ) for different species at each**  
616 **site, using daily averages.**

617 Furthermore, we could compare the model results with offline chemical information from filter samples collected  
618 in the submicron aerosol fraction at four sites in 2018: [within the CARA program](#). These filter samples were  
619 collected daily from March 15<sup>th</sup> to April 29<sup>th</sup>, 2018 in Talence, from February 16<sup>th</sup> to April 1<sup>st</sup> in Poitiers, from  
620 January 1<sup>st</sup> to January 23<sup>rd</sup>, from May 13<sup>th</sup> to May 27<sup>th</sup>, and from September 19<sup>th</sup> to September 22<sup>nd</sup> in Lyon, as  
621 well as every 4 hours from July 5<sup>th</sup> to July 27<sup>th</sup> in Marseille-Longchamp. They were analyzed in the laboratory for  
622 their organic carbon (OC), elemental carbon (EC), SO<sub>4</sub>, NO<sub>3</sub>, and NH<sub>4</sub> loadings. Figure [S4-S12](#) illustrates the  
623 comparison between model simulations and either online or offline observations, for these four sites with respect  
624 to OA, NO<sub>3</sub>, NH<sub>4</sub>, SO<sub>4</sub>, and eBC.

625 A higher correlation is observed between simulations and ACSM observations for OA, NO<sub>3</sub>, and NH<sub>4</sub> compared  
626 to filters (with  $r^2$  values of 0.5, 0.7, and 0.6 with ACSM, as opposed to 0.24, 0.54, and 0.36 with filters,  
627 respectively). SO<sub>4</sub> and eBC show relatively similar correlations (with  $r^2$  values of 0.44 and 0.42 with ACSM and  
628 AE33, respectively, and 0.18 and 0.11 with filters, respectively), but they exhibit different slopes (the model vs.  
629 ACSM-AE33 PM<sub>1</sub> demonstrates higher slopes at 0.45 and 0.5 compared to 0.36 and 0.33 with filters). Overall, the  
630 comparison of model results with observations from ACSM and AE33 shows higher correlations than with filter  
631 analyses, emphasizing the importance of online measurements for validating air quality models.

#### 632 4 Conclusions

633 This study presents multiannual measurements of ACSM and AE33 collected at 13 (sub)urban sites that are part  
634 of the French CARA program. The datasets ranged from 1 to 6 years, between 2015 and 2021. Two of those sites  
635 are integrated into the ACTRIS European infrastructure, namely ATOLL (near Lille) and SIRTA (near Paris). The  
636 dataset contains submicron aerosol species, OA, NO<sub>3</sub>, NH<sub>4</sub>, SO<sub>4</sub>, Cl, and eBC, deconvolved into eBC<sub>ff</sub> and eBC<sub>wb</sub>.  
637 A meticulous process of quality control, technical validation, and environmental assessment was employed to  
638 validate homogeneously and rigorously the datasets. This process followed the guidelines provided by the French  
639 reference laboratory for air quality monitoring and adhered strictly to the ACTRIS standard operating procedures.  
640 This article presents a comprehensive overview of these long-term datasets, offering an analysis of the  
641 geographical disparities in PM<sub>1</sub> chemical composition, as well as the main seasonal and diel variations in fine  
642 particle content.

643 Across all sites, OA is the predominant compound, with a mean concentration of 4.7  $\mu\text{g m}^{-3}$  (43-60 %) in PM<sub>1</sub>,  
644 followed by NO<sub>3</sub> (15-30 %), SO<sub>4</sub> (8-14 %), NH<sub>4</sub> (7-13 %), and eBC (5-11 %). Stations in central and southern  
645 France exhibit higher OA mass concentrations (5.3  $\mu\text{g m}^{-3}$ ), likely attributed to more pronounced photochemical  
646 formation processes. Such secondary processes may also explain that OA is the predominant compound for the  
647 highest concentration levels in summertime at all sites. ([Figure S4](#)). Additionally, for other seasons, OA exhibits  
648 greater contributions (>55 %) during periods of elevated PM<sub>1</sub> levels in the southern half of France, while NO<sub>3</sub>  
649 contributions (>40 %) are more notable during pollution episodes at northern sites, illustrating the competing  
650 influences on the aerosol chemical composition of biomass burning emissions and favorable meteorological  
651 conditions leading to the formation of ammonium nitrate, depending on the site location.

652 Temporal variations reveal distinct seasonality in PM<sub>1</sub> chemical species. eBC<sub>wb</sub> and OA peak during wintertime,  
653 with values of around 0.3 and 5.5  $\mu\text{g m}^{-3}$ , respectively, typically associated with increased residential heating

a mis en forme : Bordure : Bas: (Pas de bordure)

654 emissions. Those values peak particularly at night, combining stronger emissions and a potentially shallower  
 655 boundary layer height, facilitating pollutant accumulation. OA also peaks in summer ( $3.5 \mu\text{g m}^{-3}$ ), typically  
 656 associated with enhanced SOA formation.  $\text{NO}_3$  peaks in late winter and early spring, correlated with a typical  
 657 increase of  $\text{NH}_3$  and favorable meteorological conditions during cold periods. Diel variations also exhibit unique  
 658 characteristics at certain sites, such as the Paris Les Halles site, where an organic peak at noon suggests a significant  
 659 contribution from cooking activities; similarly, a more pronounced rush hour enhancement at BPEst suggests a  
 660 strong role of local traffic on OA levels.

661 Furthermore, the datasets presented here serve as essential tools for evaluating and validating regional and global  
 662 air quality models. An illustrative comparison with CHIMERE is presented in this paper for 2018, encompassing  
 663 nine French sites. Generally, the model successfully simulates inorganics ( $\text{NO}_3$ ,  $\text{SO}_4$ ,  $\text{NH}_4$ ) and eBC but  
 664 underestimates OA by 46-76 %, although with a high correlation between simulations and measurements ( $r$   
 665 between 0.6 and 0.8). Notably,  $\text{NO}_3$  seems to be overestimated at the ATOLL site in northern France (57 %),  
 666 whereas it is substantially underestimated by 29-42 % at southern sites. Overall, these multi-year datasets from  
 667 French urban background sites hold significant value for the scientific community, enabling future research  
 668 endeavors, including source apportionment studies, trend analyses, and epidemiological and health-related  
 669 investigations.

670 **Data availability**

671 ACSM and AE33 datasets for SIRTA and ATOLL (Villeneuve d'Ascq) are available in the EBAS database  
 672 (<https://ebas.nilu.no/>). Other measurements are available on this open link  
 673 (<https://zenodo.org/records/10790143><https://zenodo.org/records/13318298>) (Chebaicheb et al., 2024).

674 **Author contributions**

<b>Data curation &amp; Formal analysis</b>	Mélo die Chatain, Benjamin Chazeau, Hasna Chebaicheb, Jean-Eudes Petit, Shouwen Zhang
<b>Funding acquisition</b>	Olivier Favez, Véronique Riffault
<b>Investigation</b>	Hasna Chebaicheb
<b>Methodology</b>	Hasna Chebaicheb
<b>Resources</b>	Gregory Abbou, Alexia Baudic, Mélo die Chatain, Benjamin Chazeau, Florian Couvidat, Raphaële Falhun, Florie Francony, Gregory Gille, Didier Grenier, Nicolas Marchand, Jean-Eudes Petit, Cyril Ratier, Véronique Riffault, Romain Vidaud, Shouwen Zhang
<b>Supervision</b>	Joel F. de Brito, Olivier Favez, Caroline Marchand, Véronique Riffault
<b>Validation</b>	Joel F. de Brito, Olivier Favez, Caroline Marchand, Véronique Riffault
<b>Visualization</b>	Hasna Chebaicheb
<b>Writing – original draft preparation</b>	Hasna Chebaicheb, Olivier Favez

a mis en forme : Bordure : Bas: (Pas de bordure)

a mis en forme : Bordure : Bas: (Pas de bordure)

a mis en forme : Français (France)

a mis en forme le tableau

a mis en forme : Français (France)

a mis en forme : Français (France)

a mis en forme : Français (France)

a mis en forme : Français (France)

a mis en forme : Français (France)

## Writing – review & editing

All co-authors

### 675 Funding

676 This work was notably supported by the French Ministry of Environment, through direct funding of activities  
677 achieved by the AASQAs and the LCSQA in the frame of the CARA program. SIRTA observations have been  
678 partly funded by the H2020 ACTRIS-2 project under grant agreement No 654109 as well as in the frame of the  
679 CNRS-INSU long-term monitoring aerosol program SNO CLAP as a component of the ACTRIS French Research  
680 Instructure. Measurements conducted at ATOLL are also part of the Labex CaPPA project (ANR-11-LABX-0005-  
681 01), and the CLIMIBIO and ECRIN projects, both also funded by the Regional Council “Hauts-de-France” and  
682 the European Regional Development Fund (ERDF). Observations at the Marseille Longchamp supersite benefited  
683 from complementary financial support from the PACA region (PRISM project; grant n° 2017\_08809).

a mis en forme : Bordure : Bas: (Pas de bordure)

### 684 Acknowledgments

685 The authors are deeply grateful to many technicians, engineers, and scientists working in the AASQAs as well as  
686 at Ineris, IMT Nord Europe, LSCE, and LCE for their past and current involvement in the long-term operation of  
687 the monitors and data handling at the sites investigated in the present study. Authors cannot cite each of them  
688 exhaustively but strongly hope they will all recognize themselves here.

a mis en forme : Bordure : Bas: (Pas de bordure)

689 **Conflicts of Interest.** The authors declare no conflict of interest.

### 690 References

691 Allan, J. D., Delia, A. E., Coe, H., Bower, K. N., Alfarra, M. R., Jimenez, J. L., Middlebrook, A. M., Drewnick,  
692 F., Onasch, T. B., Canagaratna, M. R., Jayne, J. T., and Worsnop, D. R.: A generalised method for the extraction  
693 of chemically resolved mass spectra from Aerodyne aerosol mass spectrometer data, *J. Aerosol Sci.*, 35, 909–922,  
694 <https://doi.org/10.1016/j.jaerosci.2004.02.007>, 2004.

a mis en forme : Bordure : Bas: (Pas de bordure)

695 Alastuey, A., Querol, X., García, M., Trechera, P., Savadkoohi, M., Karanasiou, A., Minguillón, M. C., Fiebig,  
696 M., Dallénbach, K. R., Salameh, T., Sauvage, S., and Petäjä, T.: Deliverable D1 (D1.1): Guidelines, datasets of  
697 non-regulated pollutants incl. metadata, methods, 2022.

698 [Amodeo, T., 2024. Guide méthodologique pour la surveillance des PM10 et PM2.5 dans l'air ambiant par méthode  
699 optique FIDAS \(révision 2023\) | LCSQA. \[https://www.lcsqa.org/fr/rapport/guide-methodologique-pour-la-  
700 surveillance-des-pm10-et-pm25-dans-lair-ambiant-par-methode-0\]\(https://www.lcsqa.org/fr/rapport/guide-methodologique-pour-la-surveillance-des-pm10-et-pm25-dans-lair-ambiant-par-methode-0\) \(accessed 8.13.24\).](#)

701 Bond, T. C., Doherty, S. J., Fahey, D. W., Forster, P. M., Berntsen, T., DeAngelo, B. J., Flanner, M. G., Ghan, S.,  
702 Kärcher, B., Koch, D., Kinne, S., Kondo, Y., Quinn, P. K., Sarofim, M. C., Schultz, M. G., Schulz, M.,  
703 Venkataraman, C., Zhang, H., Zhang, S., Bellouin, N., Guttikunda, S. K., Hopke, P. K., Jacobson, M. Z., Kaiser,  
704 J. W., Klimont, Z., Lohmann, U., Schwarz, J. P., Shindell, D., Storelvmo, T., Warren, S. G., and Zender, C. S.:  
705 Bounding the role of black carbon in the climate system: A scientific assessment, *J. Geophys. Res. Atmospheres*,  
706 118, 5380–5552, <https://doi.org/10.1002/jgrd.50171>, 2013.



707 Bressi, M., Cavalli, F., Putaud, J. P., Fröhlich, R., Petit, J.-E., Aas, W., Äijälä, M., Alastuey, A., Allan, J. D.,  
708 Aurela, M., Berico, M., Bougiatioti, A., Bukowiecki, N., Canonaco, F., Crenn, V., Dusanter, S., Ehn, M., Elsassner,  
709 M., Flentje, H., Graf, P., Green, D. C., Heikkinen, L., Hermann, H., Holzinger, R., Hueglin, C., Keernik, H.,  
710 Kiendler-Scharr, A., Kubelová, L., Lunder, C., Maasikmets, M., Makeš, O., Malaguti, A., Mihalopoulos, N.,  
711 Nicolas, J. B., O'Dowd, C., Ovadnevaite, J., Petralia, E., Poulain, L., Priestman, M., Riffault, V., Ripoll, A.,  
712 Schlag, P., Schwarz, J., Sciare, J., Slowik, J., Sosedova, Y., Stavroulas, I., Teinmaa, E., Via, M., Vodička, P.,  
713 Williams, P. I., Wiedensohler, A., Young, D. E., Zhang, S., Favez, O., Minguillón, M. C., and Prevot, A. S. H.: A  
714 European aerosol phenomenology - 7: High-time resolution chemical characteristics of submicron particulate  
715 matter across Europe, *Atmospheric Environ.* X, 10, 100108, <https://doi.org/10.1016/j.aeaoa.2021.100108>, 2021.

716 Canagaratna, M. r., Jayne, J. t., Jimenez, J. l., Allan, J. d., Alfarra, M. r., Zhang, Q., Onasch, T. b., Drewnick, F.,  
717 Coe, H., Middlebrook, A., Delia, A., Williams, L. r., Trimborn, A. m., Northway, M. j., DeCarlo, P. f., Kolb, C.  
718 e., Davidovits, P., and Worsnop, D. r.: Chemical and microphysical characterization of ambient aerosols with the  
719 aerodyne aerosol mass spectrometer, *Mass Spectrom. Rev.*, 26, 185–222, <https://doi.org/10.1002/mas.20115>,  
720 2007.

721 Canonaco, F., Slowik, J. G., Baltensperger, U., and Prévôt, A. S. H.: Seasonal differences in oxygenated organic  
722 aerosol composition: implications for emissions sources and factor analysis, *Atmospheric Chem. Phys.*, 15, 6993–  
723 7002, <https://doi.org/10.5194/acp-15-6993-2015>, 2015.

724 Chazeau, B., Temime-Roussel, B., Gille, G., Mesbah, B., D'Anna, B., Wortham, H., and Marchand, N.:  
725 Measurement report: Fourteen months of real-time characterisation of the submicronic aerosol and its atmospheric  
726 dynamics at the Marseille–Longchamp supersite, *Atmospheric Chem. Phys.*, 21, 7293–7319,  
727 <https://doi.org/10.5194/acp-21-7293-2021>, 2021.

728 Chazeau ~~et al.~~, B., El Haddad, I., Canonaco, F., Temime-Roussel, B., D'Anna, B., Gille, G., Mesbah, B., Prévôt,  
729 A.S.H., Wortham, H., Marchand, N., 2022. Organic aerosol source apportionment by using rolling positive matrix  
730 factorization: Application to a Mediterranean coastal city. *Atmospheric environment* ~~Environment~~: X, 14, 100176.  
731 <https://doi.org/10.1016/j.aeaoa.2022.100176>

732 Chebaicheb, H., F. de Brito, J., Chen, G., Tison, E., Marchand, C., Prévôt, A. S. H., Favez, O., and Riffault, V.:  
733 Investigation of four-year chemical composition and organic aerosol sources of submicron particles at the ATOLL  
734 site in northern France, *Environ. Pollut.*, 330, 121805, <https://doi.org/10.1016/j.envpol.2023.121805>, 2023.

735 Chebaicheb, H ~~et al.~~, Phenomenology of organic aerosol multi-annual source apportionment at 12 urban and peri-  
736 urban sites in France, in preparation.

737 Chebaicheb, H., Ferreira De Brito, J., Amodeo, T., Couvidat, F., Petit, J.-E., Tison, E., Abbou, G., Alexia, B.,  
738 Chatain, M., Chazeau, B., Marchand, N., Falhun, R., Francony, F., Ratier, C., Grenier, D., Vidaud, R., Zhang, S.,  
739 Gille, G., Meunier, L., Marchand, C., Riffault, V., and Favez, O.: Multi-year high time resolution measurements  
740 of fine PM at 13 sites of the French Operational Network (CARA program),  
741 <https://doi.org/10.5281/zenodo.4079043>, 2024 [13318298](https://doi.org/10.5281/zenodo.13318298).

a mis en forme : Espace Avant : 0 pt

742 Chen, G., Canonaco, F., Tobler, A., Aas, W., Alastuey, A., Allan, J., Atabakhsh, S., Aurela, M., Baltensperger,  
743 U., Bougiatioti, A., De Brito, J. F., Ceburnis, D., Chazeau, B., Chebaicheb, H., Daellenbach, K. R., Ehn, M., El  
744 Haddad, I., Eleftheriadis, K., Favez, O., Flentje, H., Font, A., Fossom, K., Freney, E., Gini, M., Green, D. C.,  
745 Heikkinen, L., Herrmann, H., Kalogridis, A.-C., Keernik, H., Lhotka, R., Lin, C., Lunder, C., Maasikmets, M.,  
746 Manousakas, M. I., Marchand, N., Marin, C., Marmureanu, L., Mihalopoulos, N., Močnik, G., Nęcki, J., O'Dowd,  
747 C., Ovadnevaite, J., Peter, T., Petit, J.-E., Pikridas, M., Matthew Platt, S., Pokorná, P., Poulain, L., Priestman, M.,  
748 Riffault, V., Rinaldi, M., Róžański, K., Schwarz, J., Sciare, J., Simon, L., Skiba, A., Slowik, J. G., Sosedova, Y.,  
749 Stavroulas, I., Styszko, K., Teinmaa, E., Timonen, H., Tremper, A., Vasilescu, J., Via, M., Vodička, P.,  
750 Wiedensohler, A., Zografou, O., Cruz Minguillón, M., and Prévôt, A. S. H.: European aerosol phenomenology –  
751 8: Harmonised source apportionment of organic aerosol using 22 Year-long ACSM/AMS datasets, *Environ. Int.*,  
752 166, 107325, <https://doi.org/10.1016/j.envint.2022.107325>, 2022.

753 [Campagne 2021 d'étalonnage et de comparaison inter-laboratoire \(CIL\) des Q-ACSM | LCSQA:](https://www.lcsqa.org/fr/rapport/campagne-2021-detallonnage-et-de-comparaison-inter-laboratoire-cil-des-q-acsm)  
754 [https://www.lcsqa.org/fr/rapport/campagne-2021-detallonnage-et-de-comparaison-inter-laboratoire-cil-des-q-](https://www.lcsqa.org/fr/rapport/campagne-2021-detallonnage-et-de-comparaison-inter-laboratoire-cil-des-q-acsm)  
755 [acsm](https://www.lcsqa.org/fr/rapport/campagne-2021-detallonnage-et-de-comparaison-inter-laboratoire-cil-des-q-acsm), last access: 24 October 2023.

a mis en forme : Français (France)

756 Cholakian, A., Beekmann, M., Colette, A., Coll, I., Siour, G., Sciare, J., Marchand, N., Couvidat, F., Pey, J., Gros,  
757 V., Sauvage, S., Michoud, V., Sellegri, K., Colomb, A., Sartelet, K., Langley DeWitt, H., Elser, M., Prévôt, A. S.  
758 H., Szidat, S., and Dulac, F.: Simulation of fine organic aerosols in the western Mediterranean area during the  
759 ChArMEX 2013 summer campaign, *Atmospheric Chem. Phys.*, 18, 7287–7312, [https://doi.org/10.5194/acp-18-](https://doi.org/10.5194/acp-18-7287-2018)  
760 [7287-2018](https://doi.org/10.5194/acp-18-7287-2018), 2018.

761 Chrit, M., Sartelet, K., Sciare, J., Pey, J., Marchand, N., Couvidat, F., Sellegri, K., and Beekmann, M.: Modelling  
762 organic aerosol concentrations and properties during ChArMEX summer campaigns of 2012 and 2013 in the  
763 western Mediterranean region, *Atmospheric Chem. Phys.*, 17, 12509–12531, [https://doi.org/10.5194/acp-17-](https://doi.org/10.5194/acp-17-12509-2017)  
764 [12509-2017](https://doi.org/10.5194/acp-17-12509-2017), 2017.

765 Ciarelli, G., Aksoyoglu, S., Crippa, M., Jimenez, J.-L., Nemitz, E., Sellegri, K., Äijälä, M., Carbone, S., Mohr, C.,  
766 O'Dowd, C., Poulain, L., Baltensperger, U., and Prévôt, A. S. H.: Evaluation of European air quality modelled by  
767 CAMx including the volatility basis set scheme, *Atmospheric Chem. Phys.*, 16, 10313–10332,  
768 <https://doi.org/10.5194/acp-16-10313-2016>, 2016.

769 Couvidat, F. and Sartelet, K.: The Secondary Organic Aerosol Processor (SOAP v1.0) model: a unified model  
770 with different ranges of complexity based on the molecular surrogate approach, *Geosci. Model Dev.*, 8, 1111–  
771 1138, <https://doi.org/10.5194/gmd-8-1111-2015>, 2015.

772 Couvidat, Florian, [et](#) Bertrand Bessagnet. 2021. « Role of ecosystem-atmosphere exchanges of semi-volatile  
773 organic compounds in organic aerosol formation ». *Atmospheric Environment* 263 (octobre): 118541.  
774 <https://doi.org/10.1016/j.atmosenv.2021.118541>.

a mis en forme : Français (France)

775 Couvidat, Florian, Bertrand Bessagnet, Marta Garcia-Vivanco, Elsa Real, Laurent Menut, et Augustin Colette.  
776 2018. « Development of an Inorganic and Organic Aerosol Model (CHIMERE 2017β v1.0): Seasonal and Spatial

777 Evaluation over Europe». *Geoscientific Model Development* 11 (1): 165-94. [https://doi.org/10.5194/gmd-11-165-](https://doi.org/10.5194/gmd-11-165-2018)  
778 2018.

779 Crenn, V., Sciare, J., Croteau, P.L., Verlhac, S., Fröhlich, R., Belis, C.A., Aas, W., Äijälä, M., Alastuey, A.,  
780 Artiñano, B., Baisnée, D., Bonnaire, N., Bressi, M., Canagaratna, M., Canonaco, F., Carbone, C., Cavalli, F., Coz,  
781 E., Cubison, M.J., Esser-Gietl, J.K., Green, D.C., Gros, V., Heikkinen, L., Herrmann, H., Lunder, C., Minguillón,  
782 M.C., Močnik, G., O'Dowd, C.D., Ovadnevaite, J., Petit, J.-E., Petralia, E., Poulain, L., Priestman, M., Riffault,  
783 V., Ripoll, A., Sarda-Estève, R., Slowik, J.G., Setyan, A., Wiedensohler, A., Baltensperger, U., Prévôt, A.S.H.,  
784 Jayne, J.T., Favez, O., 2015. ACTRIS ACSM intercomparison – Part 1: Reproducibility of concentration and  
785 fragment results from 13 individual Quadrupole Aerosol Chemical Speciation Monitors (Q-ACSM) and  
786 consistency with co-located instruments. *Atmospheric Measurement Techniques* 8, 5063–5087.  
787 <https://doi.org/10.5194/amt-8-5063-2015>.

788 Crenn, V., Fronval, I., Petitprez, D., Riffault, V., 2017. Fine particles sampled at an urban background site and an  
789 industrialized coastal site in Northern France — Part 1: Seasonal variations and chemical characterization. *Sci.*  
790 *Total Environ.* 578, 203–218.  
791 <https://doi.org/10.1016/j.scitotenv.2015.11.165><https://doi.org/10.1016/j.scitotenv.2015.11.165>.

792 Cuesta-Mosquera, A., Močnik, G., Drinovec, L., Müller, T., Pfeifer, S., Minguillón, M.C., Briel, B., Buckley, P.,  
793 Dudoitis, V., Fernández-García, J., Fernández-Amado, M., Ferreira De Brito, J., Riffault, V., Flentje, H.,  
794 Heffernan, E., Kalivitis, N., Kalogridis, A.-C., Keernik, H., Marmureanu, L., Luoma, K., Marinoni, A., Pikridas,  
795 M., Schauer, G., Serfozo, N., Servomaa, H., Titos, G., Yus-Díez, J., Ziola, N., Wiedensohler, A., 2021.  
796 Intercomparison and characterization of 23 Aethalometers under laboratory and ambient air conditions: procedures  
797 and unit-to-unit variabilities. *Atmospheric Measurement Techniques* 14, 3195–3216. [https://doi.org/10.5194/amt-](https://doi.org/10.5194/amt-14-3195-2021)  
798 [14-3195-2021](https://doi.org/10.5194/amt-14-3195-2021).

799 Daellenbach, K. R., Bozzetti, C., Křepelová, A., Canonaco, F., Wolf, R., Zotter, P., Fermo, P., Crippa, M., Slowik,  
800 J. G., Sosedova, Y., Zhang, Y., Huang, R.-J., Poulain, L., Szidat, S., Baltensperger, U., El Haddad, I., and Prévôt,  
801 A. S. H.: Characterization and source apportionment of organic aerosol using offline aerosol mass spectrometry,  
802 *Atmospheric Meas. Tech.*, 9, 23–39, <https://doi.org/10.5194/amt-9-23-2016>, 2016.

803 Drinovec, L., Močnik, G., Zotter, P., Prévôt, A. S. H., Ruckstuhl, C., Coz, E., Rupakheti, M., Sciare, J., Müller,  
804 T., Wiedensohler, A., and Hansen, A. D. A.: The “dual-spot” Aethalometer: an improved measurement of aerosol  
805 black carbon with real-time loading compensation, *Atmospheric Meas. Tech.*, 8, 1965–1979,  
806 <https://doi.org/10.5194/amt-8-1965-2015>, 2015.

807 Dupont, J.-C., Haefelin, M., Badosa, J., Elias, T., Favez, O., Petit, J. E., Meleux, F., Sciare, J., Crenn, V., and  
808 Bonne, J. L.: Role of the boundary layer dynamics effects on an extreme air pollution event in Paris, *Atmos.*  
809 *Environ.*, 141, 571–579, <https://doi.org/10.1016/j.atmosenv.2016.06.061>, 2016.

810 European Environment Agency, 2023. Harm to human health from air pollution in Europe: burden of disease 2023.  
811 <https://www.eea.europa.eu/publications/harm-to-human-health-from-air-pollution> (accessed 3.4.24).

a mis en forme : Non souligné, Couleur de police : Automatique

a mis en forme : Non souligné, Couleur de police : Automatique

a mis en forme : Français (France)

a mis en forme : Espace Avant : 12 pt, Après : 0 pt

812 Favez, O., Cachier, H., Sciare, J., and Le Moulec, Y.: Characterization and contribution to PM<sub>2.5</sub> of semi-volatile  
813 aerosols in Paris (France), *Atmos. Environ.*, 41, 7969–7976, <https://doi.org/10.1016/j.atmosenv.2007.09.031>,  
814 2007.

815 Favez, O., El Haddad, I., Piot, C., Boréave, A., Abidi, E., Marchand, N., Jaffrezo, J.-L., Besombes, J.-L.,  
816 Personnaz, M.-B., Sciare, J., Wortham, H., George, C., and D'Anna, B.: Inter-comparison of source apportionment  
817 models for the estimation of wood burning aerosols during wintertime in an Alpine city (Grenoble, France),  
818 *Atmospheric Chem. Phys.*, 10, 5295–5314, <https://doi.org/10.5194/acp-10-5295-2010>, 2010.

819 Favez, O., Weber, S., Petit, J.-E., Alleman, L., Y., Albinet, A., Riffault, V., Chazeau, B., Amodeo, T., Salameh, D.,  
820 Zhang, Y., Srivastava, D., Samaké, A., Aujay-Plouzeau, R., Papin, A., Bonnaire, N., Boullanger, C., Chatain, M.,  
821 Chevrier, F., Detournay, A., ~~and~~ [Dominik-Sègue, M., Falhun, R., Garbin, C., Ghersi, V., Grignion, G.,  
822 Levigoureux, G., Pontet, S., Rangognio, J., Zhang, S., Besombes, J.-L., Conil, S., Uzu, G., Savarino, J., Marchand,  
823 N., Gros, V., Marchand, C., Jaffrezo, J.-L., Leoz-Garziandia, E., 2021](#). Overview of the French Operational  
824 Network for In Situ Observation of PM Chemical Composition and Sources in Urban Environments (CARA  
825 Program). [Atmosphere 12, 207](#). <https://doi.org/10.20944/preprints202101.0182.v1>, [2021-3390/atmos12020207](https://doi.org/10.20944/preprints202101.0182.v1).

826 Flentje, H., Mattis, I., Kipling, Z., Rémy, S., and Thomas, W.: Evaluation of ECMWF IFS-AER (CAMS)  
827 operational forecasts during cycle 41r1–46r1 with calibrated ceilometer profiles over Germany, *Geosci. Model*  
828 *Dev.*, 14, 1721–1751, <https://doi.org/10.5194/gmd-14-1721-2021>, 2021.

829 Foret, G., Michoud, V., Kotthaus, S., Petit, J.-E., Baudic, A., Siour, G., Kim, Y., Doussin, J.-F., Dupont, J.-C.,  
830 Formenti, P., Gaimoz, C., Ghersi, V., Gratien, A., Gros, V., Jaffrezo, J.-L., Haefelin, M., Kreitz, M., Ravetta, F.,  
831 Sartelet, K., Simon, L., Té, Y., Uzu, G., Zhang, S., Favez, O., and Beekmann, M.: The December 2016 extreme  
832 weather and particulate matter pollution episode in the Paris region (France), *Atmos. Environ.*, 291, 119386,  
833 <https://doi.org/10.1016/j.atmosenv.2022.119386>, 2022.

834 [Forster, P.M., Smith, C.J., Walsh, T., Lamb, W.F., Lamboll, R., Hauser, M., Ribes, A., Rosen, D., Gillett, N.,  
835 Palmer, M.D., Rogelj, J., von Schuckmann, K., Seneviratne, S.I., Trewin, B., Zhang, X., Allen, M., Andrew, R.,  
836 Birt, A., Borger, A., Boyer, T., Broersma, J.A., Cheng, L., Dentener, F., Friedlingstein, P., Gutiérrez, J.M.,  
837 Gütschow, J., Hall, B., Ishii, M., Jenkins, S., Lan, X., Lee, J.-Y., Morice, C., Kadow, C., Kennedy, J., Killick, R.,  
838 Minx, J.C., Naik, V., Peters, G.P., Pirani, A., Pongratz, J., Schleussner, C.-F., Szopa, S., Thorne, P., Rohde, R.,  
839 Rojas Corradi, M., Schumacher, D., Vose, R., Zickfeld, K., Masson-Delmotte, V., Zhai, P., 2023](#). Indicators of  
840 [Global Climate Change 2022: annual update of large-scale indicators of the state of the climate system and human  
841 influence](#). *Earth System Science Data 15, 2295–2327*. <https://doi.org/10.5194/essd-15-2295-2023>.

842 Fortems-Cheiney, A., Dufour, G., Hamaoui-Lague, L., Foret, G., Siour, G., Van Damme, M., Meleux, F., Coheur,  
843 P.-F., Clerbaux, C., Clarisse, L., Favez, O., Wallasch, M., and Beekmann, M.: Unaccounted variability in NH<sub>3</sub>  
844 agricultural sources detected by IASI contributing to European spring haze episode, *Geophys. Res. Lett.*, 43, 5475–  
845 5482, <https://doi.org/10.1002/2016GL069361>, 2016.

846 Freney, E., Zhang, Y., Croteau, P., Amodeo, T., Williams, L., Truong, F., Petit, J.-E., Sciare, J., Sarda-Esteve, R.,  
847 Bonnaire, N., Arumae, T., Aurela, M., Bougiatioti, A., Mihalopoulos, N., Coz, E., Artinano, B., Crenn, V., Elste,

848 T., Heikkinen, L., Poulain, L., Wiedensohler, A., Herrmann, H., Priestman, M., Alastuey, A., Stavroulas, I., Tobler,  
849 A., Vasilescu, J., Zanca, N., Canagaratna, M., Carbone, C., Flentje, H., Green, D., Maasikmets, M., Marmureanu,  
850 L., Minguillon, M. C., Prevot, A. S. H., Gros, V., Jayne, J., and Favez, O.: The second ACTRIS inter-comparison  
851 (2016) for Aerosol Chemical Speciation Monitors (ACSM): Calibration protocols and instrument performance  
852 evaluations, *Aerosol Sci. Technol.*, 53, 830–842, <https://doi.org/10.1080/02786826.2019.1608901>, 2019.

853 Fuzzi, S., Baltensperger, U., Carslaw, K., Decesari, S., Denier van der Gon, H., Facchini, M. C., Fowler, D., Koren,  
854 I., Langford, B., Lohmann, U., Nemitz, E., Pandis, S., Riipinen, I., Rudich, Y., Schaap, M., Slowik, J. G.,  
855 Spracklen, D. V., Vignati, E., Wild, M., Williams, M., and Gilardoni, S.: Particulate matter, air quality and climate:  
856 lessons learned and future needs, *Atmospheric Chem. Phys.*, 15, 8217–8299, [https://doi.org/10.5194/acp-15-8217-](https://doi.org/10.5194/acp-15-8217-2015)  
857 2015, 2015.

858 Heikkinen, L., Äijälä, M., Daellenbach, K. R., Chen, G., Garmash, O., Aliaga, D., Graeffe, F., Rätty, M., Luoma,  
859 K., Aalto, P., Kulmala, M., Petäjä, T., Worsnop, D., and Ehn, M.: Eight years of sub-micrometre organic aerosol  
860 composition data from the boreal forest characterized using a machine-learning approach, *Atmospheric Chem.*  
861 *Phys.*, 21, 10081–10109, <https://doi.org/10.5194/acp-21-10081-2021>, 2021.

862 Jacobson, M. Z.: Strong radiative heating due to the mixing state of black carbon in atmospheric aerosols, *Nature*,  
863 409, 695–697, <https://doi.org/10.1038/35055518>, 2001.

864 Janssen, N. A. H., Hoek, G., Simic, -Lawson Milena, Fischer, P., van, B. L., ten, B. H., Keuken, M., Atkinson, R.  
865 W., Anderson, H. R., Brunekreef, B., and Cassee, F. R.: Black Carbon as an Additional Indicator of the Adverse  
866 Health Effects of Airborne Particles Compared with PM10 and PM2.5, *Environ. Health Perspect.*, 119, 1691–  
867 1699, <https://doi.org/10.1289/ehp.1003369>, 2011.

868 Kiendler-Scharr, A., Mensah, A.A., Friese, E., Topping, D., Nemitz, E., Prevot, A.S.H., Äijälä, M., Allan, J.,  
869 Canonaco, F., Canagaratna, M., Carbone, S., Crippa, M., Dall'Osto, M., Day, D.A., De Carlo, P., Di Marco, C.F.,  
870 Elbern, H., Eriksson, A., Freney, E., Hao, L., Herrmann, H., Hildebrandt, L., Hillamo, R., Jimenez, J.L.,  
871 Laaksonen, A., McFiggans, G., Mohr, C., O'Dowd, C., Otjes, R., Ovadnevaite, J., Pandis, S.N., Poulain, L.,  
872 Schlag, P., Sellegri, K., Swietlicki, E., Tiitta, P., Vermeulen, A., Wahner, A., Worsnop, D., Wu, H.-C., 2016.  
873 Ubiquity of organic nitrates from nighttime chemistry in the European submicron aerosol. *Geophys. Res. Lett.* 43,  
874 7735–7744. <https://doi.org/10.1002/2016GL069239>.

875 Kuenen, J., Dellaert, S., Visschedijk, A., Jalkanen, J.-P., Super, I., and Denier van der Gon, H.: CAMS-REG-v4:  
876 a state-of-the-art high-resolution European emission inventory for air quality modelling, *Earth Syst. Sci. Data*, 14,  
877 491–515, <https://doi.org/10.5194/essd-14-491-2022>, 2022.

878 P. Laj, C. L. Myhre, V. Riffault, V. Amiridis, H. Fuchs, K. Eleftheriadis, T. Petäjä, N. Kivekäs, E. Juurola, G.  
879 Saponaro, S. Philippin, C. Cornacchia, L. Alados Arboledas, H. Baars, A. Claude, M. De Mazière, B. Dils, L. Eder  
880 Murberg, M. Fiebig, M. Haefelin, H. Herrmann, K. Höhler, N. Illmann, A. Kreuter, E. Ludewig, E. Marinou, O.  
881 Möhler, L. Mona, D. Nicolae, E. O'connor, R. M. Petracca Altieri, B. Picquet-Varrault, B. Popsichal, J.-P. Putaud,  
882 S. Reimann, T. Salameh, N. Siomos, I. Stachlewska, D. Van Pinxteren, K. A. Voudouri, U. Wandiger, A.  
883 Wiedensohler, A. Apituley, A. Comeron, M. Gysel-Beer, N. Mihalopoulos, N. Nikolova, A. Pietruczuk, S.

884 Sauvage, J. Sciare, H. Skov, T. Svendby, E. Swietlicki, D. Tonev, G. Vaughan, V. Zdimal, U. Baltensperger, J.-F.  
885 Doussin, M. Kulmala, G. Pappalardo, S. Sorvari Sundet, M. Vana, Aerosol, Cloud and Trace Gases Research  
886 Infrastructure - ACTRIS, the European research infrastructure supporting atmospheric science, in revision for  
887 Bulletin of the American Meteorological Society.

888 Lanz, V. A., Prévôt, A. S. H., Alfarra, M. R., Weimer, S., Mohr, C., DeCarlo, P. F., Gianini, M. F. D., Hueglin,  
889 C., Schneider, J., Favez, O., D'Anna, B., George, C., and Baltensperger, U.: Characterization of aerosol chemical  
890 composition with aerosol mass spectrometry in Central Europe: an overview, *Atmospheric Chem. Phys.*, **10**,  
891 10453–10471, <https://doi.org/10.5194/acp-10-10453-2010>, 2010.

892 LCSQA: Guide méthodologique pour la mesure du « Black Carbon » par Aethalomètre multi longueur d'onde  
893 AE33 dans l'air ambiant (Version 2020), 2020.

894 LCSQA: CAHIER DES CHARGES POUR L'ETALONNAGE DES Q-ACSM, 2022.

895 [Liu, P.S.K., Deng, R., Smith, K.A., Williams, L.R., Jayne, J.T., Canagaratna, M.R., Moore, K., Onasch, T.B.,](#)  
896 [Worsnop, D.R., Deshler, T., 2007. Transmission Efficiency of an Aerodynamic Focusing Lens System:](#)  
897 [Comparison of Model Calculations and Laboratory Measurements for the Aerodyne Aerosol Mass Spectrometer.](#)  
898 [Aerosol Science and Technology 41, 721–733. https://doi.org/10.1080/02786820701422278.](#)

899 Menut, L., Bessagnet, B., Briant, R., Cholakian, A., Couvidat, F., Mailler, S., Pennel, R., Siour, G., Tuccella, P.,  
900 Turquety, S., and Valari, M.: The CHIMERE v2020r1 online chemistry-transport model, *Geosci. Model Dev.*, **14**,  
901 6781–6811, <https://doi.org/10.5194/gmd-14-6781-2021>, 2021.

902 Middlebrook, A. M., Bahreini, R., Jimenez, J. L., and Cana-Garatna, M. R.: Evaluation of Composition-Dependent  
903 Collection Efficiencies for the Aerodyne Aerosol Mass Spectrometer using Field Data, *Aerosol Sci Technol*, **46**,  
904 258–271, 2011.

905 [Nault, B.A., Croteau, P., Jayne, J., Williams, A., Williams, L., Worsnop, D., Katz, E.F., DeCarlo, P.F.,](#)  
906 [Canagaratna, M., 2023. Laboratory evaluation of organic aerosol relative ionization efficiencies in the aerodyne](#)  
907 [aerosol mass spectrometer and aerosol chemical speciation monitor. Aerosol Science and Technology 57, 981–](#)  
908 [997. https://doi.org/10.1080/02786826.2023.2223249.](#)

909 [Nenes, A., Pandis, S.N., Pilinis, C., 1998. ISORROPIA: A New Thermodynamic Equilibrium Model for](#)  
910 [Multiphase Multicomponent Inorganic Aerosols. Aquatic Geochemistry 4, 123–152.](#)  
911 [https://doi.org/10.1023/A:1009604003981.](https://doi.org/10.1023/A:1009604003981)

912 Ng, N. L., Herndon, S. C., Trimborn, A., Canagaratna, M. R., Croteau, P. L., Onasch, T. B., Sueper, D., Worsnop,  
913 D. R., Zhang, Q., Sun, Y. L., and Jayne, J. T.: An Aerosol Chemical Speciation Monitor (ACSM) for Routine  
914 Monitoring of the Composition and Mass Concentrations of Ambient Aerosol, *Aerosol Sci. Technol.*, **45**, 780–  
915 794, <https://doi.org/10.1080/02786826.2011.560211>, 2011a.

a mis en forme : Français (France)

916 Ng, N. L., Canagaratna, M. R., Jimenez, J. L., Zhang, Q., Ulbrich, I. M., and Worsnop, D. R.: Real-Time Methods  
917 for Estimating Organic Component Mass Concentrations from Aerosol Mass Spectrometer Data, *Environ. Sci.*  
918 *Technol.*, 45, 910–916, <https://doi.org/10.1021/es102951k>, 2011b.

919 Petit, J.-E., Favez, O., Sciare, J., Crenn, V., Sarda-Estève, R., Bonnaire, N., Močnik, G., Dupont, J.-C., Haeffelin,  
920 M., and Leoz-Garziandia, E.: Two years of near real-time chemical composition of submicron aerosols in the  
921 region of Paris using an Aerosol Chemical Speciation Monitor (ACSM) and a multi-wavelength Aethalometer,  
922 *Atmospheric Chem. Phys.*, 15, 2985–3005, <https://doi.org/10.5194/acp-15-2985-2015>, 2015.

923 Petit, J.-E., Amodeo, T., Meleux, F., Bessagnet, B., Menut, L., Grenier, D., Pellan, Y., Ockler, A., Rocq, B., Gros,  
924 V., Sciare, J., and Favez, O.: Characterising an intense PM pollution episode in March 2015 in France from multi-  
925 site approach and near real time data: Climatology, variabilities, geographical origins and model evaluation,  
926 *Atmos. Environ.*, 155, 68–84, <https://doi.org/10.1016/j.atmosenv.2017.02.012>, 2017.

927 [Pieber, S.M., El Haddad, I., Slowik, J.G., Canagaratna, M.R., Jayne, J.T., Platt, S.M., Bozzetti, C., Daellenbach,](#)  
928 [K.R., Fröhlich, R., Vlachou, A., Klein, F., Dommen, J., Miljevic, B., Jiménez, J.L., Worsnop, D.R., Baltensperger,](#)  
929 [U., Prévôt, A.S.H., 2016. Inorganic Salt Interference on CO<sub>2</sub>+ in Aerodyne AMS and ACSM Organic Aerosol](#)  
930 [Composition Studies. \*Environ. Sci. Technol.\* 50, 10494–10503. <https://doi.org/10.1021/acs.est.6b01035>.](#)

931 [Poulain, L., Spindler, G., Grünler, A., Tuch, T., Stieger, B., van Pinxteren, D., Petit, J.-E., Favez, O., Herrmann,](#)  
932 [H., Wiedensohler, A., 2020. Multi-year ACSM measurements at the central European research station Melpitz](#)  
933 [\(Germany\) – Part 1: Instrument robustness, quality assurance, and impact of upper size cutoff diameter.](#)  
934 [Atmospheric Measurement Techniques 13, 4973–4994. <https://doi.org/10.5194/amt-13-4973-2020>.](#)

935 Putaud, J.-P., Raes, F., Van Dingenen, R., Brüggemann, E., Facchini, M.-C., Decesari, S., Fuzzi, S., Gehrig, R.,  
936 Hüglin, C., Laj, P., Lorbeer, G., Maenhaut, W., Mihalopoulos, N., Müller, K., Querol, X., Rodriguez, S., Schneider,  
937 J., Spindler, G., Brink, H. ten, Tørseth, K., and Wiedensohler, A.: A European aerosol phenomenology—2:  
938 chemical characteristics of particulate matter at kerbside, urban, rural and background sites in Europe, *Atmos.*  
939 *Environ.*, 38, 2579–2595, <https://doi.org/10.1016/j.atmosenv.2004.01.041>, 2004.

940 Roig Rodelas, R., Perdrix, E., Herbin, B., and Riffault, V.: Characterization and variability of inorganic aerosols  
941 and their gaseous precursors at a suburban site in northern France over one year (2015–2016), *Atmos. Environ.*,  
942 200, 142–157, <https://doi.org/10.1016/j.atmosenv.2018.11.041>, 2019.

943 Roig Rodelas, R., Chakraborty, A., Perdrix, E., Tison, E., Riffault, V., 2019. Real-time assessment of wintertime  
944 organic aerosol characteristics and sources at a suburban site in northern France. *Atmos. Environ.* 203, 48–61.  
945 <https://doi.org/10.1016/j.atmosenv.2019.01.035>.

946 Roldin, P., Ehn, M., Kurtén, T., Olenius, T., Rissanen, M. P., Sarnela, N., Elm, J., Rantala, P., Hao, L., Hyttinen,  
947 N., Heikkinen, L., Worsnop, D. R., Pichelstorfer, L., Xavier, C., Clusius, P., Öström, E., Petäjä, T., Kulmala, M.,  
948 Vehkamäki, H., Virtanen, A., Riipinen, I., and Boy, M.: The role of highly oxygenated organic molecules in the  
949 Boreal aerosol-cloud-climate system, *Nat. Commun.*, 10, 4370, <https://doi.org/10.1038/s41467-019-12338-8>,  
950 2019.

a mis en forme : Français (France)

951 Sandradewi, J., Prévôt, A. S. H., Szidat, S., Perron, N., Alfarra, M. R., Lanz, V. A., Weingartner, E., and  
952 Baltensperger, U.: Using Aerosol Light Absorption Measurements for the Quantitative Determination of Wood  
953 Burning and Traffic Emission Contributions to Particulate Matter, *Environ. Sci. Technol.*, 42, 3316–3323,  
954 <https://doi.org/10.1021/es702253m>, 2008.

955 Sartelet, K., Couvidat, F., Wang, Z., Flageul, C., and Kim, Y.: SSH-Aerosol v1.1: A Modular Box Model to  
956 Simulate the Evolution of Primary and Secondary Aerosols, *Atmosphere*, 11, 525,  
957 <https://doi.org/10.3390/atmos11050525>, 2020.

958 Saunders, S. M., Jenkin, M. E., Derwent, R. G., and Pilling, M. J.: Protocol for the development of the Master  
959 Chemical Mechanism, MCM v3 (Part A): tropospheric degradation of non-aromatic volatile organic compounds,  
960 *Atmospheric Chem. Phys.*, 3, 161–180, <https://doi.org/10.5194/acp-3-161-2003>, 2003.

961 Savadkoochi, M., Pandolfi, M., Reche, C., Niemi, J. V., Mooibroek, D., Titos, G., Green, D. C., Tremper, A. H.,  
962 Hueglin, C., Liakakou, E., Mihalopoulos, N., Stavroulas, I., Artiñano, B., Coz, E., Alados-Arboledas, L., Beddows,  
963 D., Riffault, V., De Brito, J. F., Bastian, S., Baudic, A., Colombi, C., Costabile, F., Chazeau, B., Marchand, N.,  
964 Gómez-Amo, J. L., Estellés, V., Matos, V., van der Gaag, E., Gille, G., Luoma, K., Manninen, H. E., Norman, M.,  
965 Silvergren, S., Petit, J.-E., Putaud, J.-P., Rattigan, O. V., Timonen, H., Tuch, T., Merkel, M., Weinhold, K.,  
966 Vratolis, S., Vasilescu, J., Favez, O., Harrison, R. M., Laj, P., Wiedensohler, A., Hopke, P. K., Petäjä, T., Alastuey,  
967 A., and Querol, X.: The variability of mass concentrations and source apportionment analysis of equivalent black  
968 carbon across urban Europe, *Environ. Int.*, 178, 108081, <https://doi.org/10.1016/j.envint.2023.108081>, 2023.

969 [Savadkoochi, M., Pandolfi, M., Favez, O., Putaud, J.-P., Eleftheriadis, K., Fiebig, M., Hopke, P.K., Laj, P.,](#)  
970 [Wiedensohler, A., Alados-Arboledas, L., Bastian, S., Chazeau, B., María, Á.C., Colombi, C., Costabile, F., Green,](#)  
971 [D.C., Hueglin, C., Liakakou, E., Luoma, K., Listrani, S., Mihalopoulos, N., Marchand, N., Močnik, G., Niemi,](#)  
972 [J.V., Ondráček, J., Petit, J.-E., Rattigan, O.V., Reche, C., Timonen, H., Titos, G., Tremper, A.H., Vratolis, S.,](#)  
973 [Vodička, P., Funes, E.Y., Zíková, N., Harrison, R.M., Petäjä, T., Alastuey, A., Querol, X., 2024. Recommendations](#)  
974 [for reporting equivalent black carbon \(eBC\) mass concentrations based on long-term pan-European in-situ](#)  
975 [observations. \*Environment International\* 185, 108553. <https://doi.org/10.1016/j.envint.2024.108553>.](#)

976 Schaap, M., Spindler, G., Schulz, M., Acker, K., Maenhaut, W., Berner, A., Wieprecht, W., Streit, N., Müller, K.,  
977 Brüggemann, E., Chi, X., Putaud, J.-P., Hitznerberger, R., Puxbaum, H., Baltensperger, U., and ten Brink, H.:  
978 Artefacts in the sampling of nitrate studied in the “INTERCOMP” campaigns of EUROTRAC-AEROSOL, *Atmos.*  
979 *Environ.*, 38, 6487–6496, <https://doi.org/10.1016/j.atmosenv.2004.08.026>, 2004.

980 Sun, J., Zhang, Q., Canagaratna, M. R., Zhang, Y., Ng, N. L., Sun, Y., Jayne, J. T., Zhang, X., Zhang, X., and  
981 Worsnop, D. R.: Highly time- and size-resolved characterization of submicron aerosol particles in Beijing using  
982 an Aerodyne Aerosol Mass Spectrometer, *Atmos. Environ.*, 44, 131–140,  
983 <https://doi.org/10.1016/j.atmosenv.2009.03.020>, 2010.

984 Tobler, A. K., Skiba, A., Wang, D. S., Croteau, P., Styszko, K., Nećki, J., Baltensperger, U., Slowik, J. G., and  
985 Prévôt, A. S. H.: Improved chloride quantification in quadrupole aerosol chemical speciation monitors (Q-  
986 ACSMs), *Atmospheric Meas. Tech.*, 13, 5293–5301, <https://doi.org/10.5194/amt-13-5293-2020>, 2020.



987 Tobler, A. K., Skiba, A., Canonaco, F., Močnik, G., Rai, P., Chen, G., Bartyzel, J., Zimnoch, M., Styszko, K.,  
988 Nęcki, J., Furger, M., Róžański, K., Baltensperger, U., Slowik, J. G., and Prevot, A. S. H.: Characterization of  
989 non-refractory (NR) PM<sub>1</sub> and source apportionment of organic aerosol in Kraków, Poland, *Atmospheric Chem.*  
990 *Phys.*, 21, 14893–14906, <https://doi.org/10.5194/acp-21-14893-2021>, 2021.

991 Viana, M., Kuhlbusch, T. A. J., Querol, X., Alastuey, A., Harrison, R. M., Hopke, P. K., Winiwarter, W., Vallius,  
992 M., Szidat, S., Prévôt, A. S. H., Hueglin, C., Bloemen, H., Wählin, P., Vecchi, R., Miranda, A. I., Kasper-Giebl,  
993 A., Maenhaut, W., and Hitzenberger, R.: Source apportionment of particulate matter in Europe: A review of  
994 methods and results, *J. Aerosol Sci.*, 39, 827–849, <https://doi.org/10.1016/j.jaerosci.2008.05.007>, 2008.

995 Wang, Z., Couvidat, F., and Sartelet, K.: GENerator of reduced Organic Aerosol mechanism (GENOA v1.0): an  
996 automatic generation tool of semi-explicit mechanisms, *Geosci. Model Dev.*, 15, 8957–8982,  
997 <https://doi.org/10.5194/gmd-15-8957-2022>.

998 Wang, Z., Couvidat, F., and Sartelet, K.: Implementation of a parallel reduction algorithm in the GENerator of  
999 reduced Organic Aerosol mechanisms (GENOA v2.0): Application to multiple monoterpene aerosol precursors,  
1000 *J. Aerosol Sci.*, 174, 106248, <https://doi.org/10.1016/j.jaerosci.2023.106248>, 2023.

1001 ~~Wang, Z., Couvidat, F., and Sartelet, K. (2024), Response of biogenic secondary organic aerosol formation to~~  
1002 ~~anthropogenic NOx emission mitigation. Submitted to Science of The Total Environment, 927, 172142.~~  
1003 ~~<https://doi.org/10.1016/j.scitotenv.2024.172142>.~~

1004 Watson, T. B.: Aerosol Chemical Speciation Monitor (ACSM) Instrument Handbook,  
1005 <https://doi.org/10.2172/1375336>, 2017.

1006 Wittmaack, K. and Keck, L.: Thermodesorption of aerosol matter on multiple filters of different materials for a  
1007 more detailed evaluation of sampling artifacts, *Atmos. Environ.*, 38, 5205–5215,  
1008 <https://doi.org/10.1016/j.atmosenv.2004.05.047>, 2004.

1009 WHO Air Quality Guidelines: [https://www.c40knowledgehub.org/s/article/WHO-Air-Quality-](https://www.c40knowledgehub.org/s/article/WHO-Air-Quality-Guidelines?language=en_US)  
1010 [Guidelines?language=en\\_US](https://www.c40knowledgehub.org/s/article/WHO-Air-Quality-Guidelines?language=en_US), last access: 23 January 2023.

1011 ~~Xu, W., Lambe, A., Silva, P., Hu, W., Onasch, T., Williams, L., Croteau, P., Zhang, X., Renbaum-Wolff, L.,~~  
1012 ~~Fortner, E., Jimenez, J.L., Jayne, J., Worsnop, D., Canagaratna, M., 2018. Laboratory evaluation of species-~~  
1013 ~~dependent relative ionization efficiencies in the Aerodyne Aerosol Mass Spectrometer. *Aerosol Science and*~~  
1014 ~~*Technology* 52, 626–641. <https://doi.org/10.1080/02786826.2018.1439570>.~~

1015 Zanatta, M., Gysel, M., Bukowiecki, N., Müller, T., Weingartner, E., Areskou, H., Fiebig, M., Yttri, K. E.,  
1016 Mihalopoulos, N., Kouvarakis, G., Beddows, D., Harrison, R. M., Cavalli, F., Putaud, J. P., Spindler, G.,  
1017 Wiedensohler, A., Alastuey, A., Pandolfi, M., Sellegri, K., Swietlicki, E., Jaffrezo, J. L., Baltensperger, U., and  
1018 Laj, P.: A European aerosol phenomenology-5: Climatology of black carbon optical properties at 9 regional  
1019 background sites across Europe, *Atmos. Environ.*, 145, 346–364, <https://doi.org/10.1016/j.atmosenv.2016.09.035>,  
1020 2016.

a mis en forme : Couleur de police : Noir, Français (France)

a mis en forme : Couleur de police : Noir, Français (France)

a mis en forme : Couleur de police : Noir, Français (France)

a mis en forme : Couleur de police : Noir

a mis en forme : Bordure : Haut: (Pas de bordure), Bas: (Pas de bordure), Gauche: (Pas de bordure), Droite: (Pas de bordure), Entre : (Pas de bordure)

a mis en forme : Couleur de police : Noir

a mis en forme : Couleur de police : Noir

a mis en forme : Couleur de police : Noir

a mis en forme : Couleur de police : Noir

a mis en forme : Français (France)

1021 Zhang, S., Tison, E., Dusanter, S., Beaugard, C., Gengembre, C., Augustin, P., Fourmentin, M., Delbarre, H.,  
1022 Riffault, V., 2021. Near real-time PM1 chemical composition measurements at a French urban background and  
1023 coastal site under industrial influence over more than a year: Temporal variability and assessment of sulfur-  
1024 containing emissions. *Atmos. Environ.* 244, 117960. <https://doi.org/10.1016/j.atmosenv.2020.117960>.

1025 Zhang, Y., Favez, O., Albinet, A., Canonaco, F., Truong, F., Amodeo, T., Prevot, A., Sciare, J., and Gros, V.:  
1026 Long-term measurements of the chemistry and sources of submicron aerosols at SIRTa in Paris area, France, in:  
1027 *European Aerosol Conference (EAC 2017)*, Zurich, Switzerland, 2017.

1028 Zhang, Y., Favez, O., Petit, J.-E., Canonaco, F., Truong, F., Bonnaire, N., Crenn, V., Amodeo, T., Prévôt, A. S.  
1029 H., Sciare, J., Gros, V., and Albinet, A.: Six-year source apportionment of submicron organic aerosols from near-  
1030 continuous highly time-resolved measurements at SIRTa (Paris area, France), *Atmospheric Chem. Phys.*, 19,  
1031 14755–14776, <https://doi.org/10.5194/acp-19-14755-2019>, 2019.